General Disclaimer

One or more of the Following Statements may affect this Document

- This document has been reproduced from the best copy furnished by the organizational source. It is being released in the interest of making available as much information as possible.

- This document may contain data, which exceeds the sheet parameters. It was furnished in this condition by the organizational source and is the best copy available.

- This document may contain tone-on-tone or color graphs, charts and/or pictures, which have been reproduced in black and white.

- This document is paginated as submitted by the original source.

- Portions of this document are not fully legible due to the historical nature of some of the material. However, it is the best reproduction available from the original submission.

RADAR CROSS SECTION MEASUREMENTS OF A SCALE MODEL OF THE SPACE SHUTTLE ORBITER VEHICLE

WILLIAM T. YATES
MICROWAVE BRANCH

MARCH 1978

PACIFIC MISSILE TEST CENTER
POINT MUGU, CALIFORNIA

ACKNOWLEDGMENTS

The author wishes to express his appreciation to Mr. T. W. Sheehan, Projects Support Office, National Aeronautics and Space Administration, Lyndon B. Johnson Space Center, Houston, Texas, for his assistance in this project, and to Mr. J. Pennington, Pacific Miniatures, Incorporated, Alhambra, California, for his cooperation in the development of the radar reflectivity version of the Space Shuttle Orbiter model.

Appreciation is also expressed to Messrs. R. Giesel and Y. Kobashigawa for their work in making the measurements, and to Messrs. R. Fries, D. Mensa, and E. Tetreault for their technical assistance.

TABLE OF CONTENTS

Page

SUMMARY

A series of microwave measurements was conducted to determine the radar cross section (RCS) of the Space Shuttle Orbiter vehicle at a frequency and at aspect angles applicable to re-entry radar acquisition and tracking. The measurements were performed in a microwave anechoic chamber using a 1/15th-scale model and a frequency applicable to C-band tracking radars. The data were digitally recorded and processed to yield statistical descriptions useful for prediction of orbiter re-entry detection and tracking ranges.

Analysis of the data yielded the following results for the Space Shuttle Orbiter:

1. The median RCS of the orbiter vehicle exhibited a gradual increase from approximately +10 decibels relative to 1 square meter (dBsm) at nose aspects to approximately +27 dBsm at tail aspects.

2. Large peak values of RCS at aspect angles near 90 degrees were observed in and above the yaw plane of the orbiter.

3. Smaller peak values of RCS at aspect angles near 45 degrees were observed in the yaw plane of the orbiter.

4. The dynamic range of orbiter RCS amplitude scintillation was approximately 10-15 decibels (dB).

5. The nose and tail aspect RCS values were not strongly correlated with tilt or roll angles.

6. The orbiter vehicle generally meets or exceeds proposed minimum RCS requirements for acquisition and tracking by C-band ground-based radars during re-entry.

7. Median RCS for the orbiter are summarized in the table below.

Tilt Angle (Degrees)	Roll Angle (Degrees)	Median Radar Cross Section (dBsm) Aspect Angle (Degrees)							
		0	45	90	135	180	225	270	315
0	0	9.3	17.2	30.2	22.9	28.2	20.3	44.0	17.2
-5	0	6.4	14.3	20.6	18.9	30.3	20.3	22.6	13.1
+5	0	9.1	15.1	36.1	21.3	30.7	21.4	35.8	15.0
-10	0	5.1	11.6	20.3	18.3	27.4	18.4	20.3	11.7
+10	0	12.3	17.1	36.0	21.5	31.0	21.3	36.0	17.0
0	10	11.2	15.3	35.6	19.1	29.5	21.2	21.4	12.6
0	20	5.9	11.2	30.0	19.7	31.7	17.8	15.3	10.3
0	30	10.1	11.7	26.3	19.4	32.8	18.1	15.3	10.2
0	40	11.8	12.9	27.5	19.7	27.3	16.6	22.1	14.1
0	50	6.8	13.5	31.1	20.5	25.7	15.6	15.8	8.5
0	60	13.4	14.7	30.3	18.7	28 1	18.1	15.2	13.4
0	70	12.5	15.0	30.8	19.6	28.1	19.4	19.5	14.6
0	80	11.0	15.1	34.6	19.4	29.4	19.0	27.9	14.3
0	90	10.2	14.7	32.8	19.5	25.5	21.4	35.7	15.2

INTRODUCTION

The Pacific Missile Test Center (PACMISTESTCEN) was funded by the National Aeronautics and Space Administration (NASA), Johnson Space Center, Houston, Texas, to conduct RCS measurements on a scale model of the Space Shuttle Orbiter vehicle. Authorization, funds, and work requirements were established by NASA Defense Purchase Request T-3445F of 22 August 1977.

These measurements were designed to yield results applicable to ground-based, C-band radar acquisition and tracking of the Space Shuttle Orbiter vehicle during re-entry.

Measurements were made on a 1/15th-scale model of the orbiter at roll angles from 0 to 90 degrees at intervals of 10 degrees, and at tilt angles of +10, +5, -5, and -10 degrees. The measurement frequency of 94 Gigahertz (GHz) was selected on the basis of equipment and model availability and yielded a full-scale frequency of 6.27 GHz. Vertical polarization was used for all tilt cuts and for the 0- through 50-degree roll cuts. Horizontal polarization was used for the 60- through 90-degree roll cuts. Due to target symmetry, the roll data are valid for both positive and negative roll angles. Several of the tilt cuts were measured over aspect angles more than 180 degrees but less than 360 degrees. In these cases, target symmetry allowed the missing data to be supplied by replicating corresponding portions of the measured data. Table 1 summarizes the test parameters for the RCS measurements of the Space Shuttle Orbiter model.

This report is submitted as fulfillment of project requirements.

DESCRIPTION OF MODEL

The Space Shuttle Orbiter model, shown in figures 1 through 5, is a 1/15th-scale model of molded-fiberglass shell construction manufactured by Pacific Miniatures, Incorporated, Alhambra, California. The model length is 2.27 meters, the wing span is 1.59 meters, and the height is 1.16 meters.

Major features of the orbiter are the ogival noise, flat-sided fuselage, thick wings with curved leading edges, vertical stablizer, Orbital Manuevering System (OMS) rocket engine pods, rocket engine exhaust bells, speed brake, and lifting-body curvature of the vehicle underside. The model wings, vertical stabilizer, and speed brake are removable and the cargo-bay doors may be opened. The model engine exhaust bells are made of metal.

The surface of the model, including the interior of the cargo bay, is coated with conductive silver paint to simulate the metallic construction of the vehicle. Measurements of the surface resistance were made to establish the uniformity, integrity, and conductivity of the surface coating. The actual orbiter vehicle is partially covered by various types and thickness of thermal protective system (TPS) material. Several antennas are also covered by TPS. Due to the

difficulty in modeling such materials and antennas, it was determined to model the entire orbiter surface as a metallic skin. This modeling will generally provide a minimum radar backscatter result for targets such as the orbiter (references 1 and 2).

The conductive surface of the model was overpainted with the orbiter color scheme. In addition to enhancing the appearance of the model, this paint layer provides a protective coating for the silver paint.

MEASUREMENT TECHNIQUE

The RCS measurements of the orbiter model were conducted in the small PACMISTESTCEN microwave anechoic chamber (figure 6). The chamber, approximately 5 meters high by 8 meters wide by 23 meters long, provides an electromagnetic environment approximating free space at the measurement frequency. The walls, ceiling, and floor of the chamber at lined with microwave absorber which attenuates reflections of microwave energy radiated within the chamber and isolates the chamber enclosure from microwave energy radiated externally. The model was positioned on a vertical styrofoam column extending halfway to the ceiling near one end of the chamber. The measurement equipment was located at the opposite end of the chamber, with the measurement system antennas positioned at the same level as (and approximately 18 meters from) the model. A typical equipment configuration, shown in figure 7, consists of a highly stable radio frequency (RF) energy source, a transmitting antenna, a receiving antenna, a canceling network, a receiver, and a data recording system.

The signal generated by the stable microwave source is radiated by the transmitting antenna which provides illumination of the target with field density variations of less than 2 decibels (dB). The backscattered signal, captured by the receiving antenna, is detected and recorded. In the absence of a target, a residual signal is received from chamber wall reflections and from crosstalk between antennas. This residual signal is canceled by coupling a portion of the transmitted signal into the receiver through a microwave network. The network provides amplitude and phase control of the coupled signal to effect cancellation. After canceling the residual signal, the system is calibrated in terms of absolute RCS by measuring the signal backscattered from a simple metallic shape (typically a cylinder) of known RCS. This procedure establishes a reference RCS level which provides a calibration for the subsequent model measurement. Consistent with equation (2) below, the calibration level is adjusted by the square of the scale factor to compensate for the effect of scaling. Subsequent to cancellation and calibration, the model is positioned on the column in such a way that prescribed aspects are presented to the measurement system as the column is rotated. Data are acquired as the column rotates through a complete revolution.

The theory of scale measurements requires that the wavelength be scaled by the same factor as the model in order that the ratio of target dimensions to wavelength remain constant. The measurements, performed at microwave frequencies greater than the required full-scale frequencies by a factor equal to the scale factor, yield a relative measure of RCS. Absolute calibration is obtained by measuring a metallic object of simple shape and of known RCS. The relation between the RCS of a target, σ_T, and the RCS of a scale model, σ_M, is given by the equation:

$$\sigma_T = \sigma_M \text{ (scale factor)}^2 \qquad (1)$$

which, for the measurements reported here, is

$$\sigma_T = \sigma_M (15.0)^2 = 225\ \sigma_M \qquad (2)$$

COORDINATE SYSTEMS

PACMISTESTCEN System

The coordinate system used for the measurements defines the position of the target and the positioner column with respect to the measurement system antennas. For the measurements reported here, the model was positioned on the column in such a way that the roll axis of the model was normal to the longitudinal axis of the column. The following terms describe the coordinate system, diagrammed in figure 8.

ASPECT ANGLE: The angle defining the rotation of the column about its longitudinal axis. Aspect angle is zero when the nose of the model is aligned with the midpoint between the measurement antennas. Aspect angle becomes positive with counterclockwise rotation of the column from zero, and becomes negative with clockwise rotation from zero. A 360-degree rotation of the column presents the necessary aspect angles to record one pattern.

ROLL ANGLE: The angle defining the rotation of the model about its roll axis with respect to the supporting column. Roll angle is zero when the pitch axis of the model is normal to the longitudinal axis of the column, and becomes positive with declination of the port wing.

TILT ANGLE: The angle defining the inclination of the column toward or away from the measurement site. Tilt angle is zero when the column is vertical, and positive when the column is inclined toward the measurement site.

PITCH ANGLE: The angle defining the rotation of the model about its pitch axis. Pitch angle is zero when the longitudinal or roll axis of the model is horizontal, and becomes positive with declination of the nose.

BISTATIC ANGLE: The angle subtended by the lines of sight from the target to the transmitting and receiving antennas. If the bistatic angle is essentially zero, the measurement is termed monostatic.

POLARIZATION: Polarization defines the direction of the transmitted electric field vector with respect to the chamber floor. Polarization is termed horizontal when the electric field vector is parallel to the chamber floor, and vertical when the electric field vector is normal to the chamber floor. The receiving antenna is oriented to receive backscattered energy polarized in the same direction as the transmitted energy.

NASA System

The NASA coordinate system (reference 1) differs from that used in this report. The two coordinates used are defined as follows:

AZIMUTH ANGLE: The angle in the yaw plane measured clockwise from the nose. The angles range from 0 degrees (nose) to 180 degrees (tail) and continue to 360 degrees (nose).

ELEVATION ANGLE: The angle normal to the yaw plane at a specified azimuth angle measured downward from the target yaw axis. The angles range from 0 degrees (directly over the target) to 180 degrees (directly beneath the target). An elevation angle of 90 degrees defines the yaw plane.

RCS PATTERN COVERAGE

Figure 9 illustrates the coverage provided by the measurements in this report. The axes are in NASA coordinates. The cross-hatched region indicates the desired coverage for 450 nautical mile acquisition from Pt. Pillar and Vandenberg AFB radars (reference 1). The single-hatched region shows the additional coverage desired for 150 nautical mile acquisition from San Nicolas Island and the FRC station near Edwards AFB (reference 1). The five horizontal lines (+80, +85, +90, +95, and +100 degrees elevation) illustrate the +10-, +5-, 0-, -5-, and -10-degree tilt cuts, respectively. The curved lines indicate the roll coverage from 10 to 80 degrees roll. The 0-degree roll cut is the same as the 0-degree tilt cut. The 90-degree roll cut lies on the 0-degree azimuth and 180-degree azimuth coordinate lines.

DATA ACQUISITION

The RCS of the target is digitally recorded on magnetic tape by a data acquisition system specifically designed for this purpose. The system consists of an analog-to-digital converter which is enabled by pulse outputs from a digital shaft encoder mounted on the target positioner. The data are sampled at selected angular intervals, digitized, and recorded on a seven-track incremental digital tape recorder. The format of the data allows direct access to digital computer processing.

The recording system allows a resolution of 0.1 dB, an accuracy of ±0.1 dB, a dynamic range of 80 dB, and a minimum intersample spacing of 0.01 degree.

The data were sampled at 0.02-degree intervals. All data were digitally recorded on magnetic tape and retained for future reference. Data processing was performed by an IBM 7094 computer using a library of programs specifically designed for this purpose. The graphs of processed data are reproductions from 24x images on microfiche generated with a computer-controlled Stromberg Datagraphix SD-4460 plotter.

DATA PROCESSING

The RCS of aircraft targets, observed at microwave frequencies, exhibit large, erratic fluctuations as a function of aspect angle. Figure 10 shows a typical recording of the RCS of an aircraft plotted versus aspect angle. The RCS data recorded as a function of aspect angle span a relatively large dynamic range, typically 40 to 60 dB. In order to be accurately recorded and displayed, the data are usually converted to logarithmic form. Because RCS is proportional to the echo signal power, the RCS is expressed in terms of dBsm by the relation $\sigma_{dBsm} = 10 \log \sigma_{square\ meters}$. The large fluctuations, caused by complex interference among signals backscattered from various parts of the target, preclude a concise quantitative description of the RCS. Therefore, the data must be treated statistically for the majority of applications to radar system analyses. From the wide variety of statistical processes which can be applied to the data, the following were selected to provide results of general utility.

Continuous Percentiles

A technique for smoothing fluctuations in the raw data consists of determining the cumulative probability distribution of the data contained in a small angular sector and plotting various percentiles as a function of aspect angle. The 50th percentile, termed the median value, represents the value of RCS that exceeds 50 percent of the data samples within the angular interval. Similarly, the 10th and 90th percentiles represent the values of RCS that exceed 10 and 90 percent, respectively, of the data samples. The median yields a central value of RCS, while the 10th and 90th percentiles define extreme values of RCS. Prior reports and other investigators have customarily selected an angular interval of 10 degrees. A more significant treatment consists of analyzing the statistics of the data that would be observed if the aspect angle varied randomly about a given angle. This condition is representative of the RCS behavior as a radar observes a target at a nominally fixed aspect angle with flight-induced perturbations. Data are processed by computing the percentiles of RCS resulting from aspect angle variations that are normally distributed with a standard deviation of 2 degrees. The computations, repeated as the aspect angle interval is stepped in 1-degree increments, yield a nearly continuous plot of the percentiles. Figure 11 shows a typical result of data processed by this method. The upper line superimposed on the raw data is the 90th percentile, the

center line is the 50th percentile (median), and the lower line is the 10th percentile. For clarity, the percentiles in the report are displayed separately from the raw data.

Fourth Root of RCS

In many radar system analyses, acquisition range is a variable of interest and importance. Acquisition range is related to radar system parameters and RCS of the target by the radar range equations:

$$R_{MAX} = \frac{P_T G^2 \lambda^2 \sigma}{(4\pi)^3 P_{R_{MIN}}} \tag{3}$$

where R_{MAX} = maximum acquisition range

P_T = transmitted power

$P_{R_{MIN}}$ = minimum detectable received power

G = antenna gain

λ = wavelength

σ = target RCS

Equation (3) can be rewritten to separate the radar parameters from the target RCS as:

$$R_{MAX} = \left[\frac{P_T G^2 \lambda^2}{(4\pi)^3 P_{R_{MIN}}} \right]^{1/4} \sigma^{1/4} \tag{4}$$

For a given radar with fixed parameters, the terms in the brackets comprise a lumped constant; the acquisition range is, therefore, proportional to the fourth root of RCS. A plot of the fourth root of RCS as a function of aspect angle exhibits the relative acquisition range for radars observing the target. In addition to graphically portraying the acquisition range envelopes, the fourth root of RCS provides a convenient compression of the large dynamic range of the data, thus obviating the need for expressing them in terms of dB. Figure 12 shows a typical polar plot of the fourth root of median RCS derived from the 50th percentile values described in the preceding section. Values are plotted relative to a 1 square meter target.

Anomalies in the recording process caused minor perturbations in the data at +40 degrees aspect angle on pattern 77-2581, and at +65 degrees aspect angle on pattern 77-2584. These perturbations are of very short angular extent and do not affect the conclusions of this report in any way.

RESULTS AND DISCUSSION

Aspect Angle Dependence

The median RCS of the Space Shuttle Orbiter exhibits a gradual increase as the aspect angle is increased from the nose. In general, the median nose-aspect RCS is approximately +10 dBsm, rising approximately 1 dB per 10-degree increase in aspect angle from the nose for the first 70 degrees. After the peak at 90 degrees aspect angle, the median RCS increases from approximately +15 dBsm at 120 degrees aspect to +27 dBsm at the tail, rising approximately 2 dB per 10-degree increase in aspect angle.

Large peak values of RCS, occasionally exceeding the measurement limit of +45 dBsm, occur at aspect angles normal to the longitudinal (roll) axis of the vehicle. These large values are due, at low roll angles, to reflections from the side of the fuselage, the vertical stablizer, and the OMS engine pods. At high roll angles these peaks are due to reflections from the top and bottom of the fuselage and wings. At intermediate roll angles above the yaw plane the apparent sources of the RCS peak are the fuselage and the fuselage-wing dihedral.

Lesser peaks occur at approximately 45 degrees aspect angle from the nose in the yaw plane due to reflections from the leading edge of the wings.

Values of the median RCS of the orbiter at every 45 degrees of aspect angle from the nose for each pattern are tabulated in Table 2. Plots of the 10th, 50th, and 90th percentiles and mean value of RCS of the orbiter are shown in figures 14 through 27. Polar plots of the median acquisition range relative to that for a 0 dBsm (1 square meter) target are shown in figures 28 through 41. The RCS amplitude scintillation is approximately 10 to 15 dB.

Tilt Angle Dependence

The median RCS of the Space Shuttle Orbiter is a weak function of tilt angle for the region of $\pm$10 degrees tilt. (Note that the RCS of the orbiter measured at a tilt angle of +10 degrees corresponds to a 360-degree view of the orbiter at a fixed elevation angle of 10 degrees above the yaw plane.) There is a slight decrease in median RCS for the nose and tail region at negative tilt angles. The broadside peak is prominent at 0-, +5-, and +10-degree tilt angles, but is 10 to 23 dB lower at -5- and -10-degree tilt angles. This effect is attributed to shadowing of the fuselage, OMS engine pods, and tail regions by the wings at these negative tilt angles.

Roll Angle Dependence

The median RCS of the Space Shuttle Orbiter is a weak function of roll angle. The peak at 90 degrees aspect angle is prominent at 0-, 80-, and 90-degree roll angles, but is a minor feature for roll angles where the wing shields the fuselage. At 20-, 30-, and 50-degree roll angles, the median RCS exhibits a broad minimum from 0 to 40 degrees aspect angle. This minimum is approximately 3 to 7 dB below the median RCS in this region for all other roll angles. In general, the median RCS as a function of roll angle exhibits the same values and structure described in the discussion of aspect angle dependence.

Comparison with Predicted RCS

The RCS of the Space Shuttle Orbiter has been predicted by calculations of the RCS of geometric shapes chosen to approximate the vehicle configuration (references 1 and 2). Except for regions of peak RCS, the predictions tend to underestimate the RCS values in the forward quadrant. The predictions are most accurate in the region of 60 to 75 degrees aspect angle. The predicted peak values at 45, 80, and 90 degrees aspect angle are too large. Figure 13 illustrates the difference between the measured and calculated RCS for the 0- through 90-degree aspect angle region in the yaw plane.

Applicability of Results

The results of RCS measurements of a scale model of the Space Shuttle Orbiter, as reported herein, may be used for predictions of acquisition range by C-band radars during re-entry and in-orbit tracking. These results represent a probable minimum - RCS configuration of the orbiter vehicle. Extension of these results to other vehicle configurations and frequencies is not recommended.

Acquisition of the Space Shuttle Orbiter on re-entry is subject to many constraints (references 1 through 5). However, it has been determined that an FPQ-6 radar requires a minimum RCS of +5 dBsm for detection at 450 nautical mile (reference 3). The RCS of the orbiter vehicle generally meets or exceeds this minimum requirement for acquisition and tracking by C-band ground-based radars during re-entry.

REFERENCES

1. Lockheed Electronics Company, Inc., memorandum from Y. C. Loh to J. A. Porter, NASA, EJ2, Memo No. 77-2209-086, of 11 July 1977. Subj: C-Band Radar Coverage for OFT-1 Entry Phase.

2. RCS Government Systems Division. Space Shuttle Orbiter Radar Cross Section Modeling and Simulation. Moorestown, New Jersey, 30 September 1977.

3. Lockheed Electronics Company, Inc., memorandum from C. M. Lequieu to S. W. Novosad, NASA, EJ2, Memo No. 77-2209-081, of 17 June 1977. Subj: C-Band Radar Tracking for Entry Phase of OFT Flights.

4. Lockheed Electronics Company, Inc., memorandum from C. M. Lequieu to J. A. Porter, NASA, EJ2, Memo No. 77-2209-092, of 22 July 1977. Subj: C-Band Radar Tracking Analysis.

5. Mission Planning and Analysis Division. OFT-1 Reference Flight Profile - De-orbit Through Landing. National Aeronautics and Space Administration, Lyndon B. Johnson Space Center, Houston, Texas, JSC-12957, August 1977.

Table 1. Summary of Test Parameters for Radar Cross Section Measurements of Space Shuttle Orbiter Model

Pattern	Tilt	Roll	Polarization*	Figures
77-2579	0	0	Vertical	14, 28
77-2581	-5	0	Vertical	15, 29
77-2582	+5	0	Vertical	16, 30
77-2583	-10	0	Vertical	17, 31
77-2584	+10	0	Vertical	18, 32
77-2585	0	-10	Vertical	19, 33
78-0011	0	+20	Vertical	20, 34
78-0012	0	+30	Vertical	21, 35
78-0013	0	+40	Vertical	22, 36
78-0014	0	+50	Vertical	23, 37
78-0015	0	+60	Horizontal	24, 38
78-0016	0	+70	Horizontal	25, 39
78-0018	0	+80	Horizontal	26, 40
78-0017	0	+90	Horizontal	27, 41

*Polarization is measured with respect to the anechoic chamber floor.

Table 2. Median Radar Cross Section of Space Shuttle Orbiter Model

Tilt Angle (Degrees)	Roll Angle (Degrees)	Median Radar Cross Section (dBsm) Aspect Angle (Degrees) 0	45	90	135	180	225	270	315
0	0	9.3	17.2	30.2	22.9	28.2	20.3	44.0	17.2
-5	0	6.4	14.3	20.6	18.9	30.3	20.3	22.6	13.1
+5	0	9.1	15.1	36.1	21.3	30.7	21.4	35.8	15.0
-10	0	5.1	11.6	20.3	18.3	27.4	18.4	20.3	11.7
+10	0	12.3	17.1	36.0	21.5	31.0	21.3	36.0	17.0
0	10	11.2	15.3	35.6	19.1	29.5	21.2	21.4	12.6
0	20	5.9	11.2	30.0	19.7	31.7	17.8	15.3	10.3
0	30	10.1	11.7	26.3	19.4	32.8	18.1	15.3	10.2
0	40	11.8	12.9	27.5	19.7	27.3	16.6	22.1	14.1
0	50	6.8	13.5	31.1	20.5	25.7	15.6	15.8	8.5
0	60	13.4	14.7	30.3	18.7	28.1	18.1	15.2	13.4
0	70	12.5	15.0	30.8	19.6	28.1	19.4	19.5	14.6
0	80	11.0	15.1	34.6	19.4	29.4	19.0	27.9	14.3
0	90	10.2	14.7	32.8	19.5	25.5	21.4	35.7	15.2

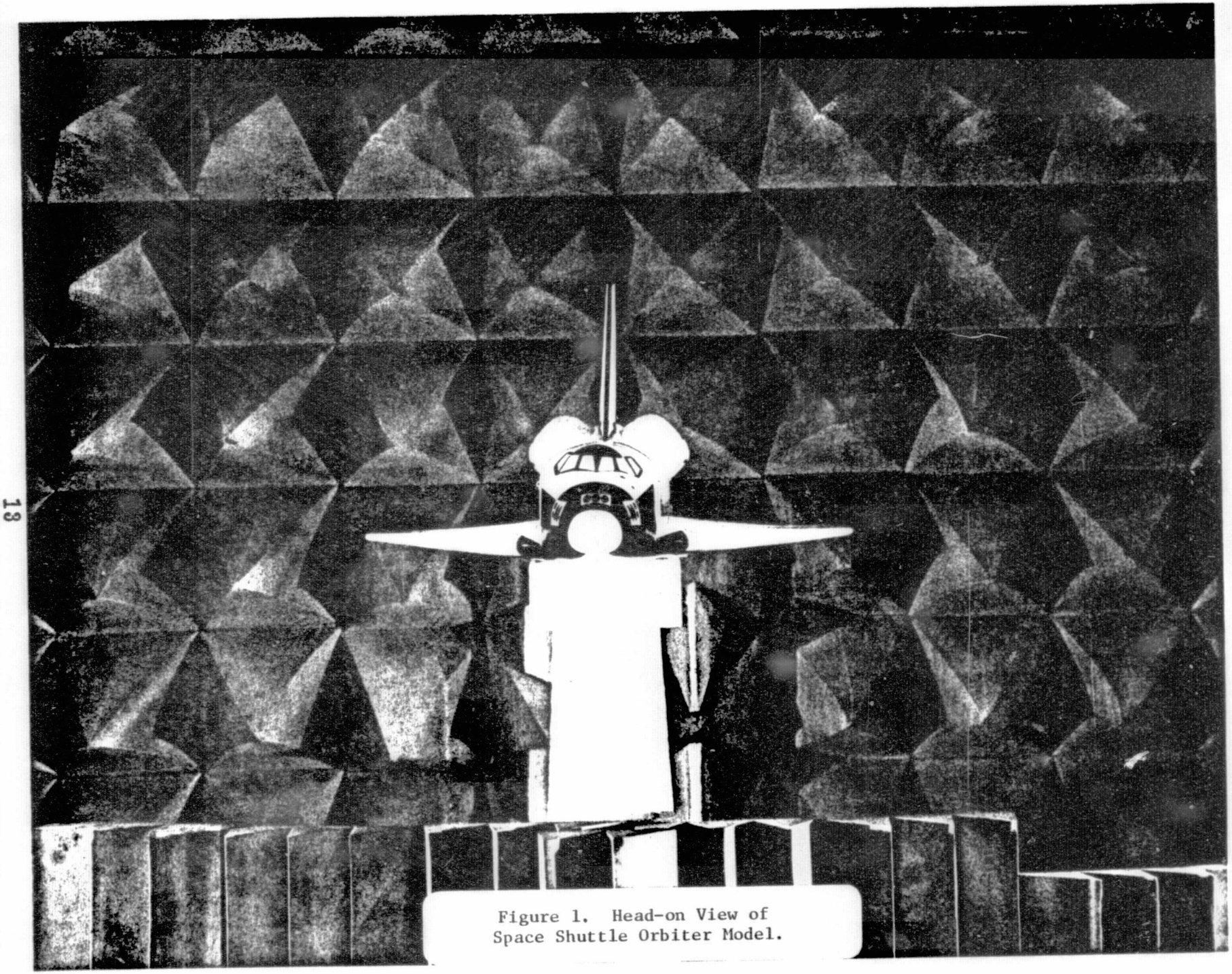

Figure 1. Head-on View of
Space Shuttle Orbiter Model.

Figure 2. Side View of
Space Shuttle Orbiter Model.

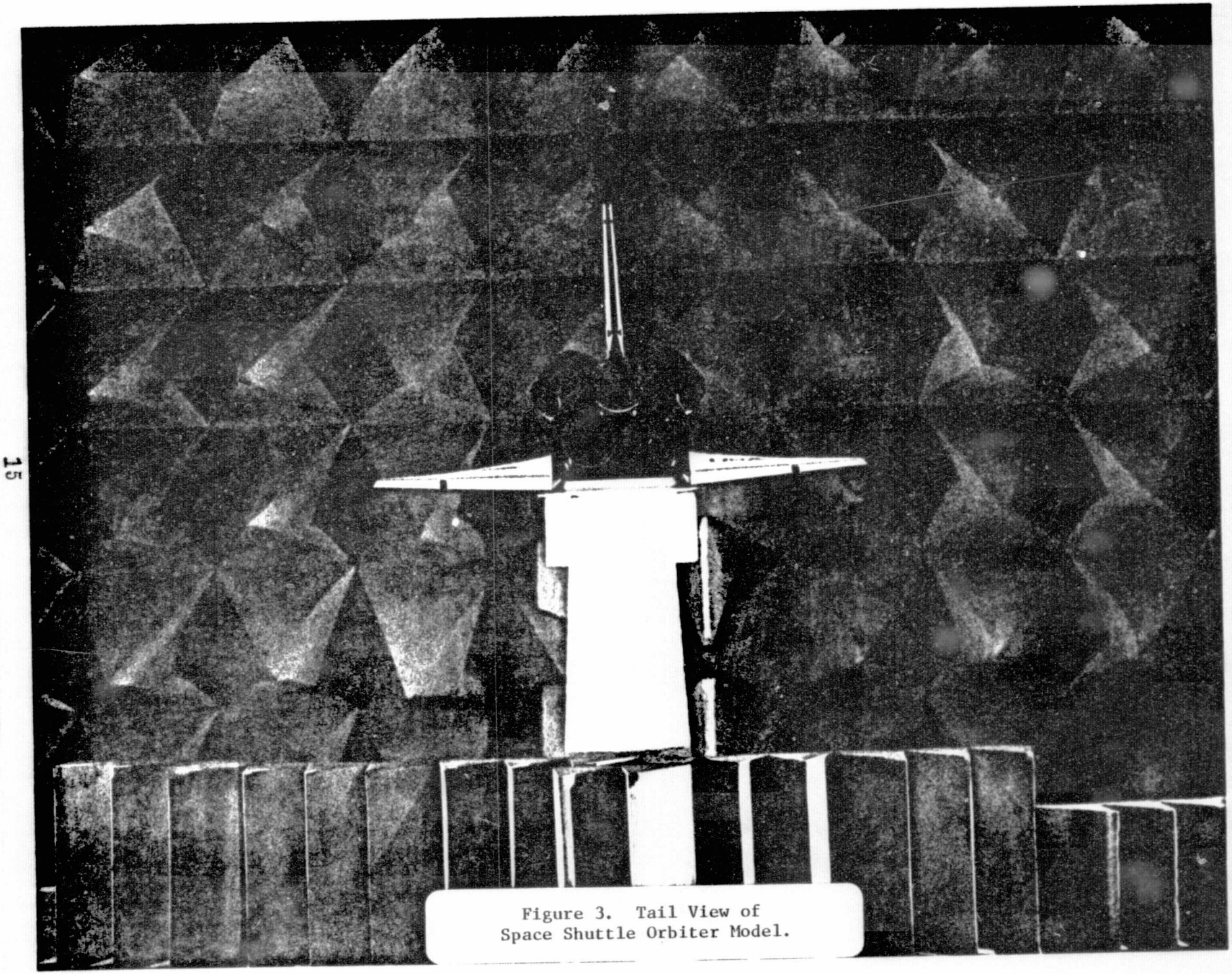

Figure 3. Tail View of
Space Shuttle Orbiter Model.

Figure 4. Nose Section of
Space Shuttle Orbiter Model.

Figure 5. Tail Section of Space Shuttle Orbiter Model.

Figure 6. The 5- by 8- by 23-Meter Microwave Anechoic Chamber of the Pacific Missile Test Center.

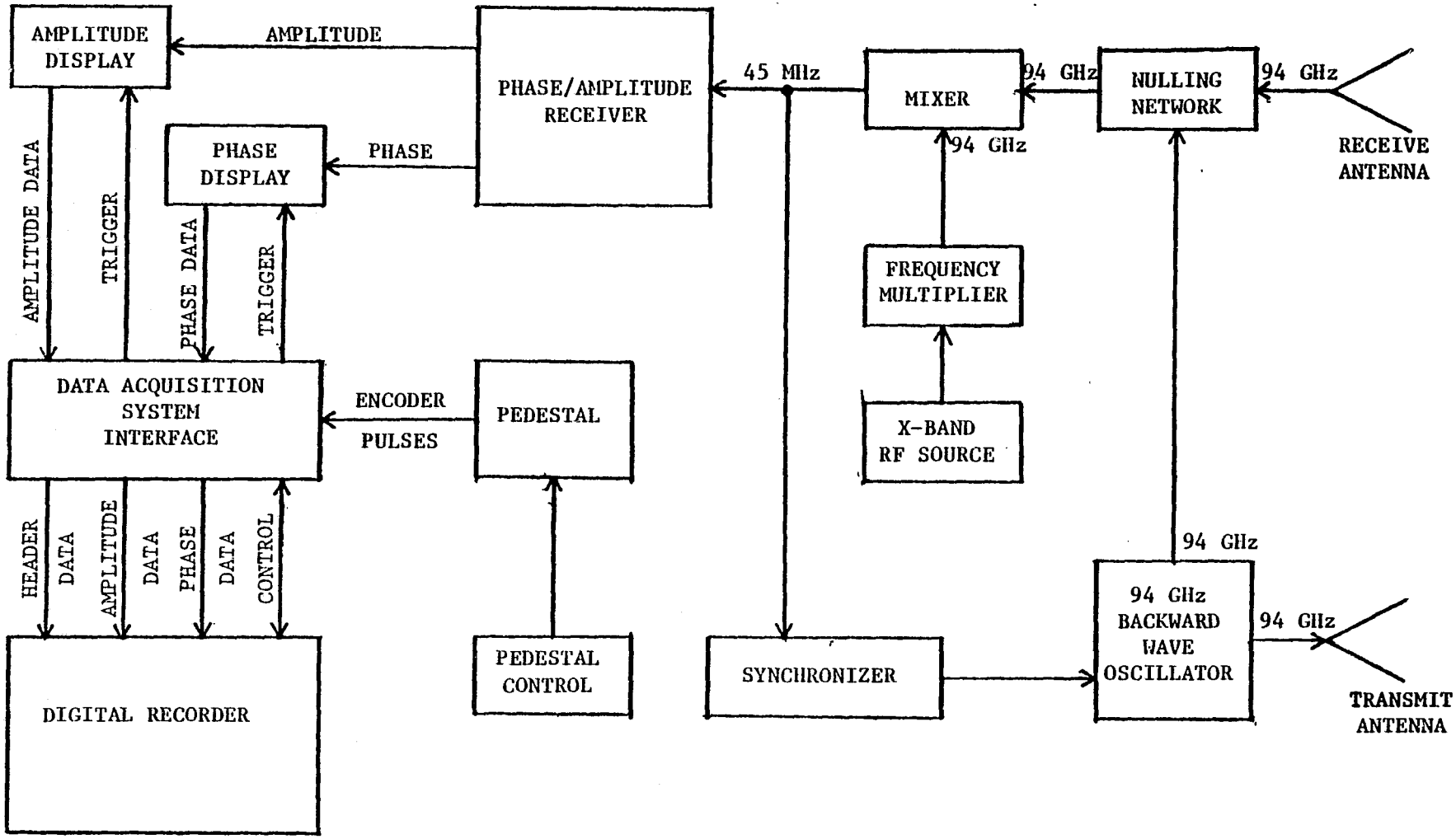

Figure 7. Block Diagram of Typical 94 GHz Continuous-Wave Radar Cross Section Measurement System.

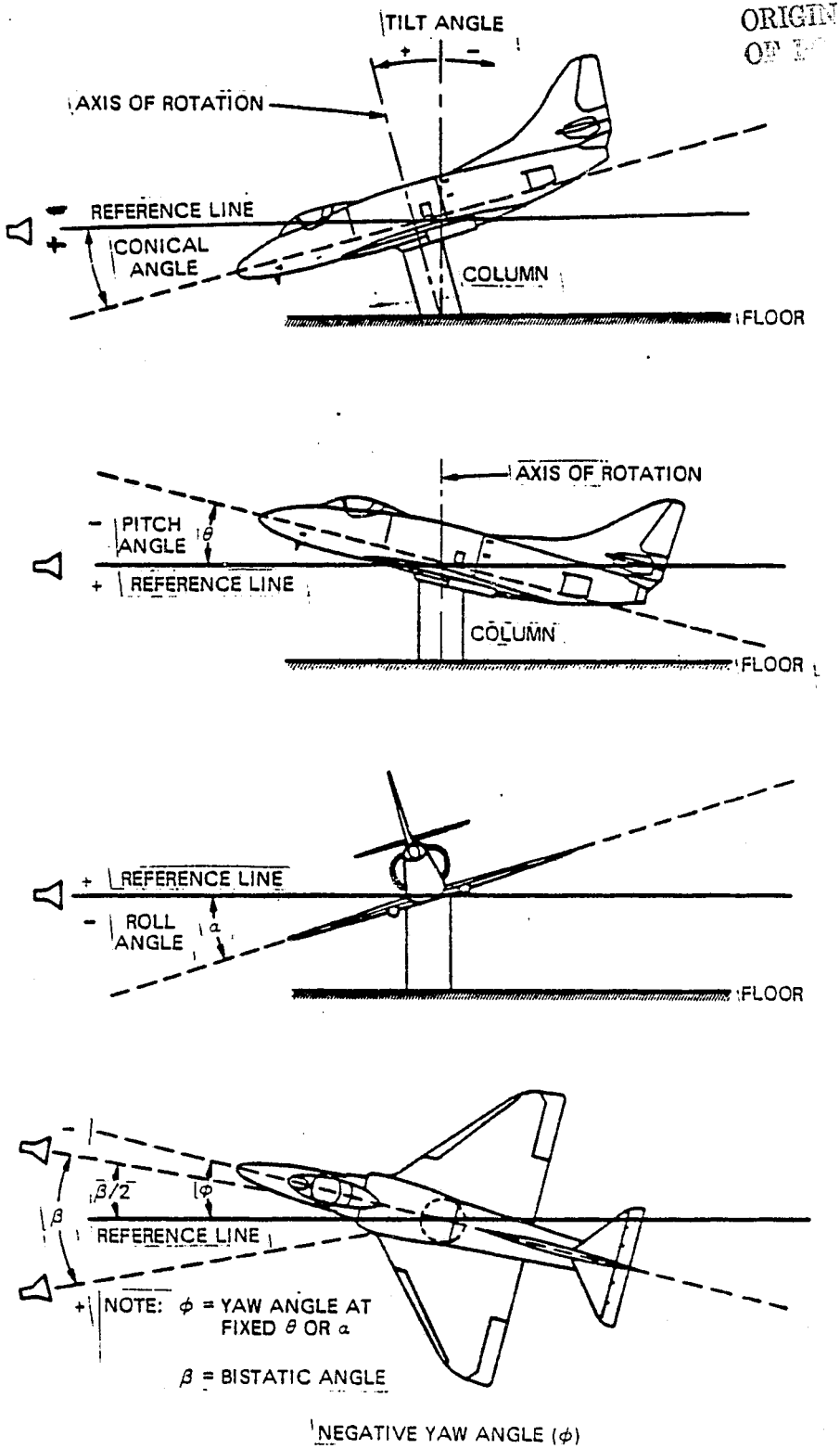

Figure 8. Coordinate System Used for Pacific Missile Test Center Anechoic Chamber Measurements.

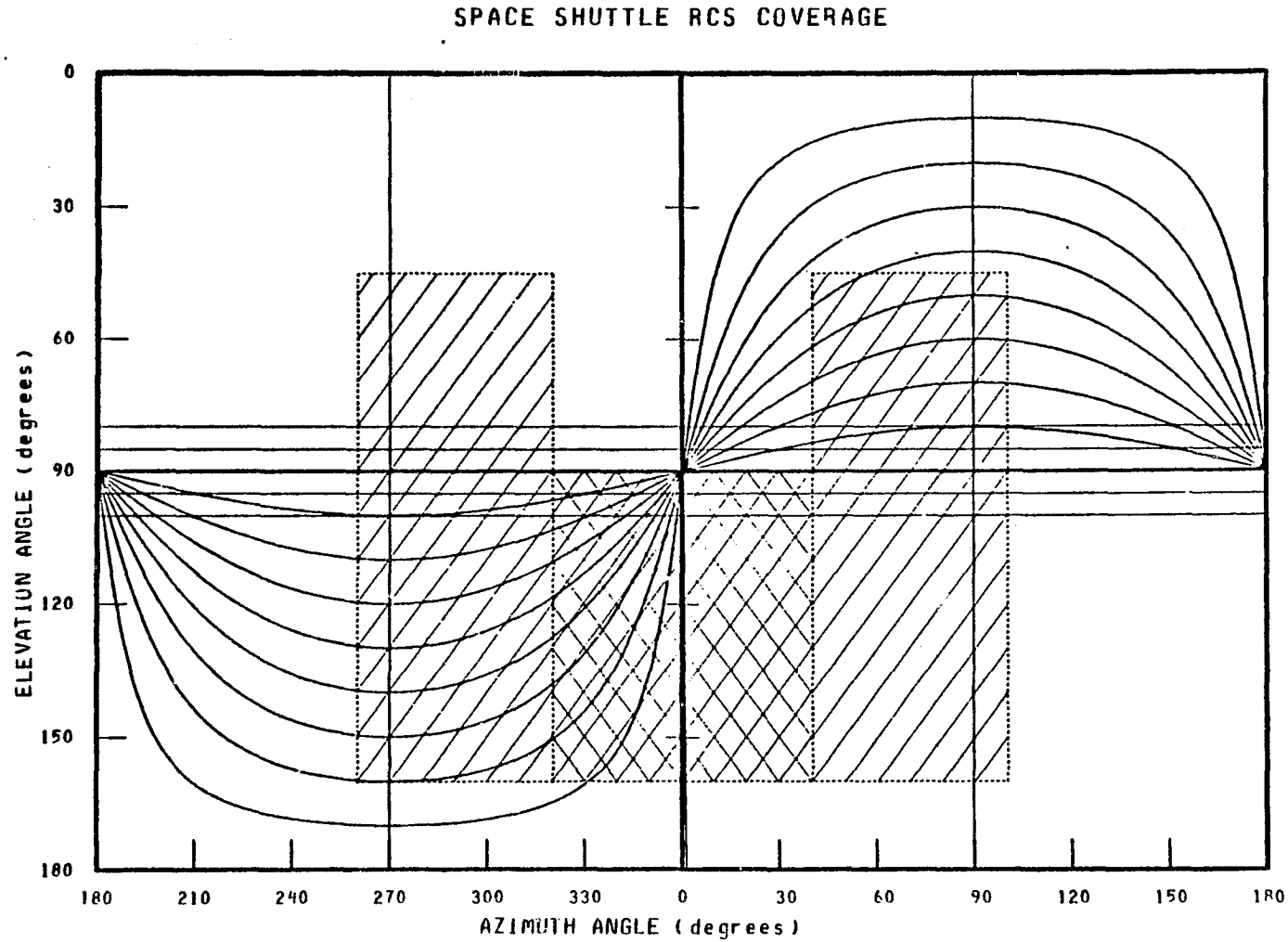

Figure 9. Radar Cross Section Pattern Coverage (NASA Coordinates).

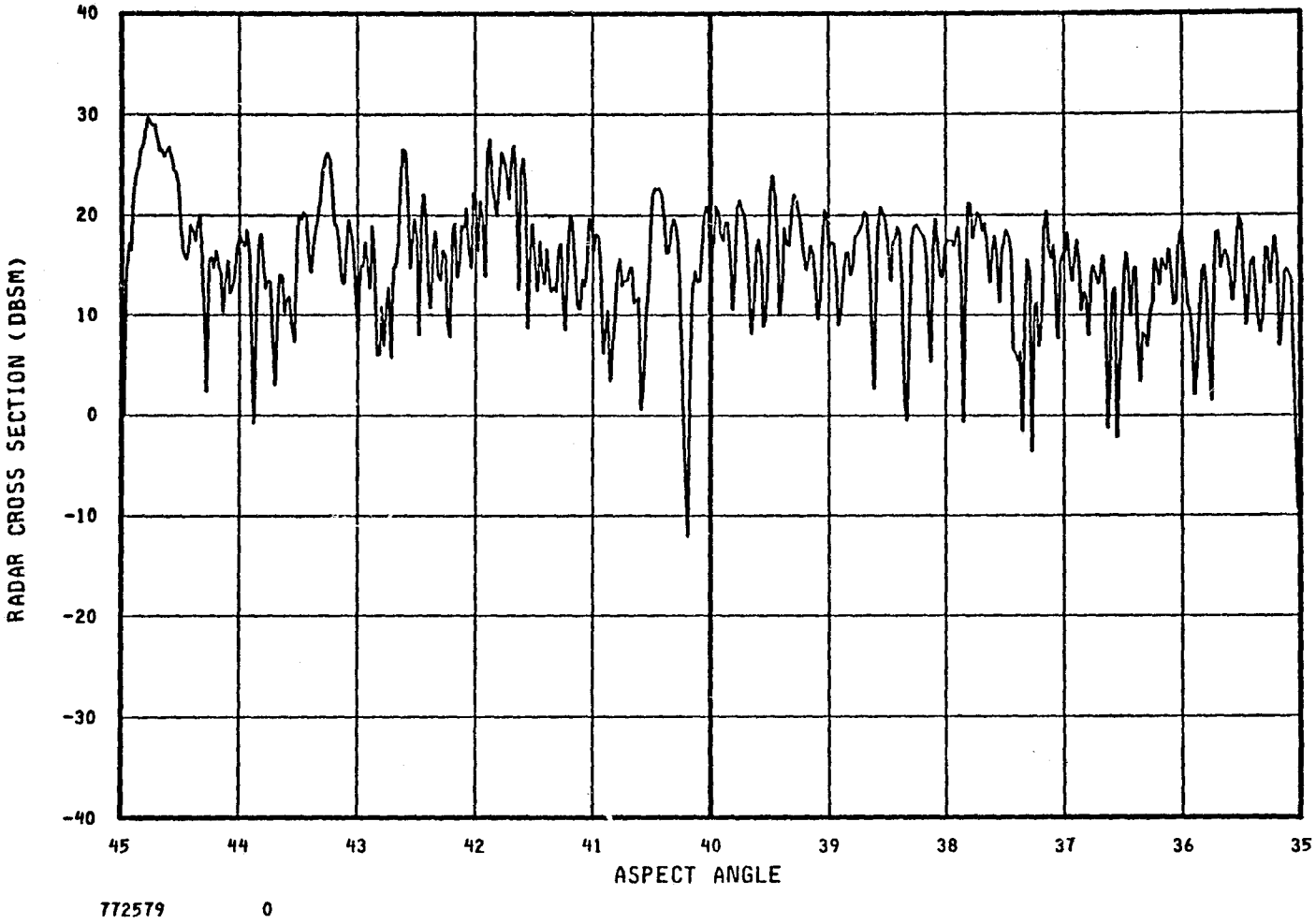

Figure 10. Typical 10-Degree Segment of Radar Cross Section Pattern.

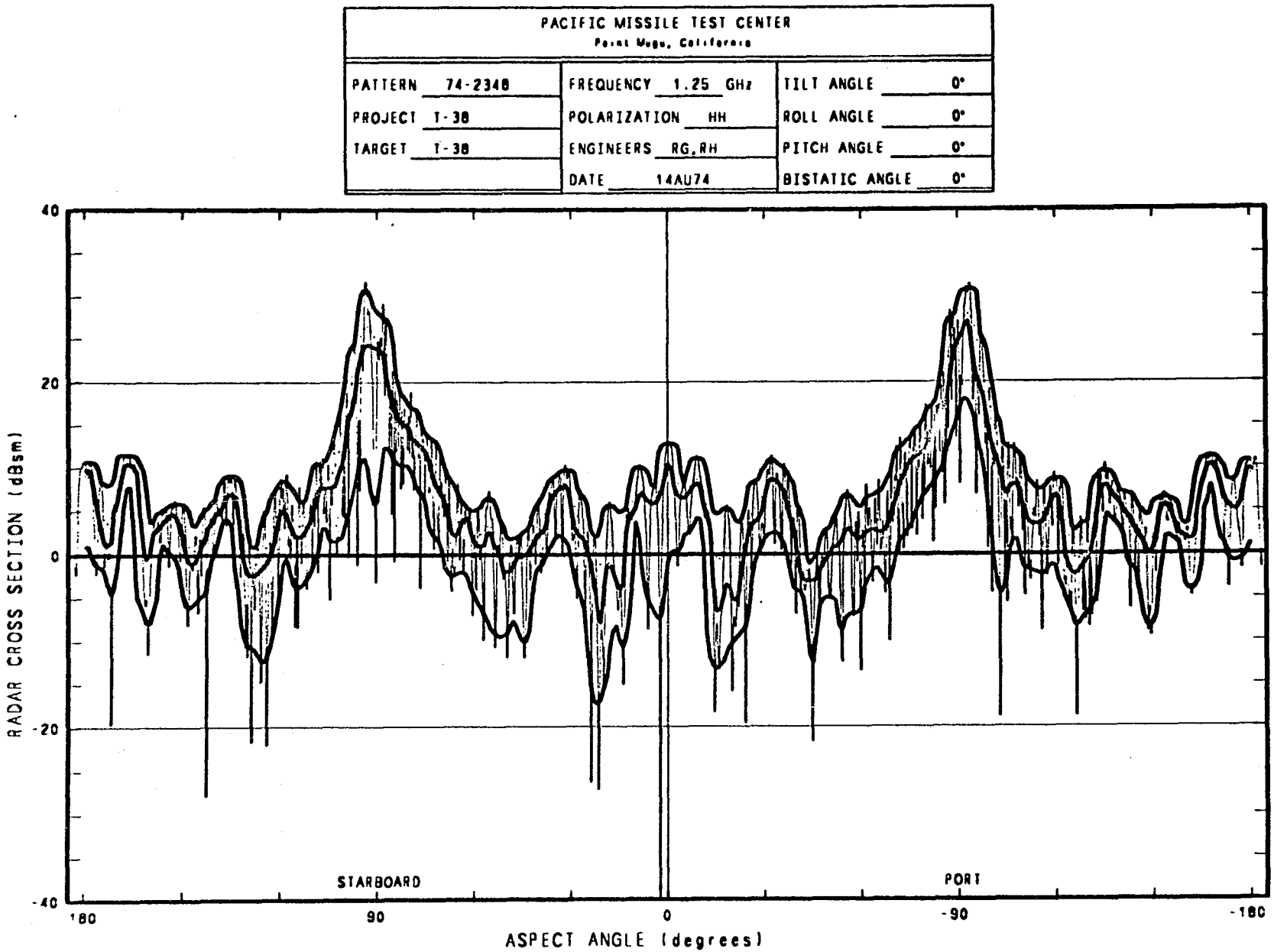

Figure 11. 10th, 50th, and 90th Percentiles Superimposed on Radar Cross Section Pattern.

PACIFIC MISSILE TEST CENTER Point Mugu, California		
PATTERN 78-0013 00	FREQUENCY 6.27 GHz	TILT ANGLE 0°
PROJECT SPACESHUTTLE	POLARIZATION VV	ROLL ANGLE + 40°
TARGET ORBITER	ENGINEERS WY,RG,YK	PITCH ANGLE 0°
	DATE 05JA78	BISTATIC ANGLE 0°

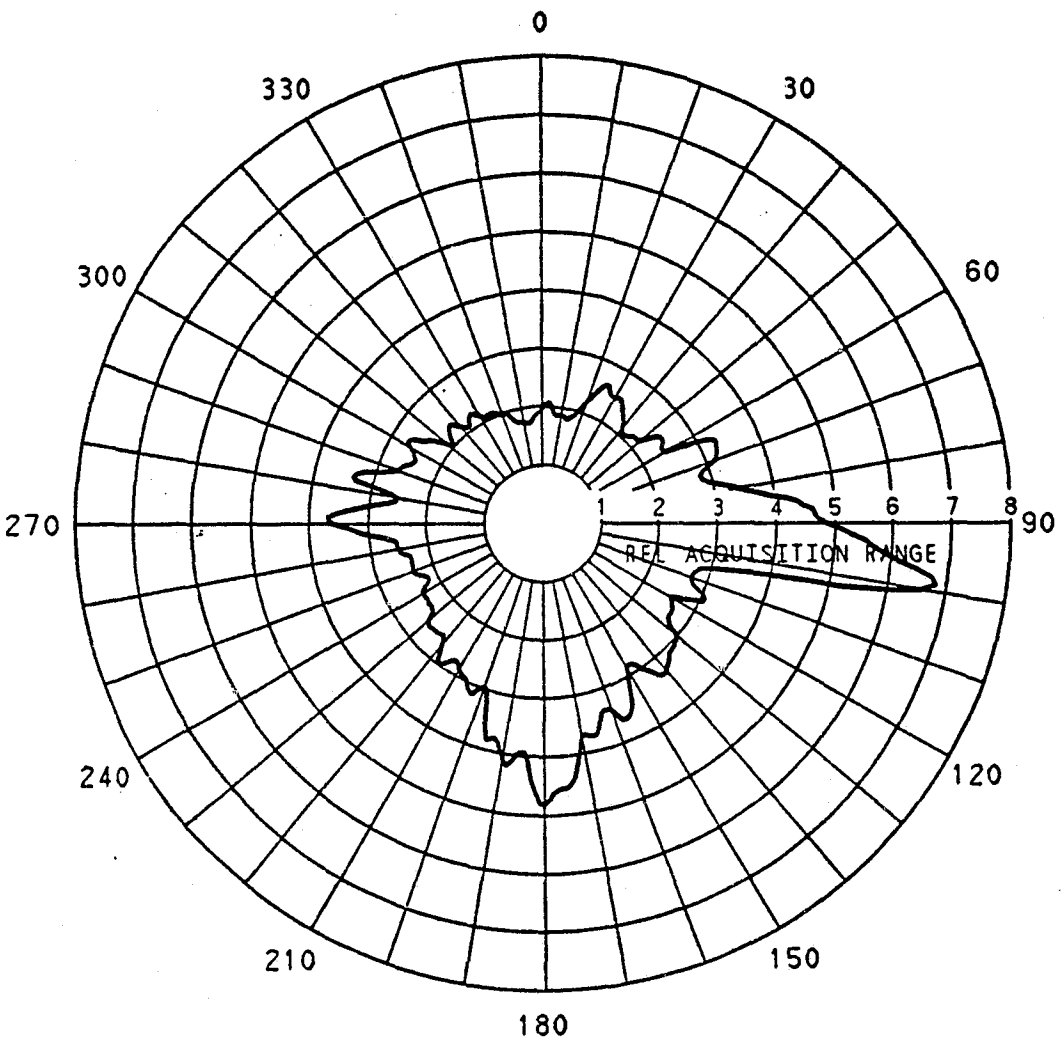

Figure 12. Polar Plot of Fourth Root of Median Radar Cross Section.

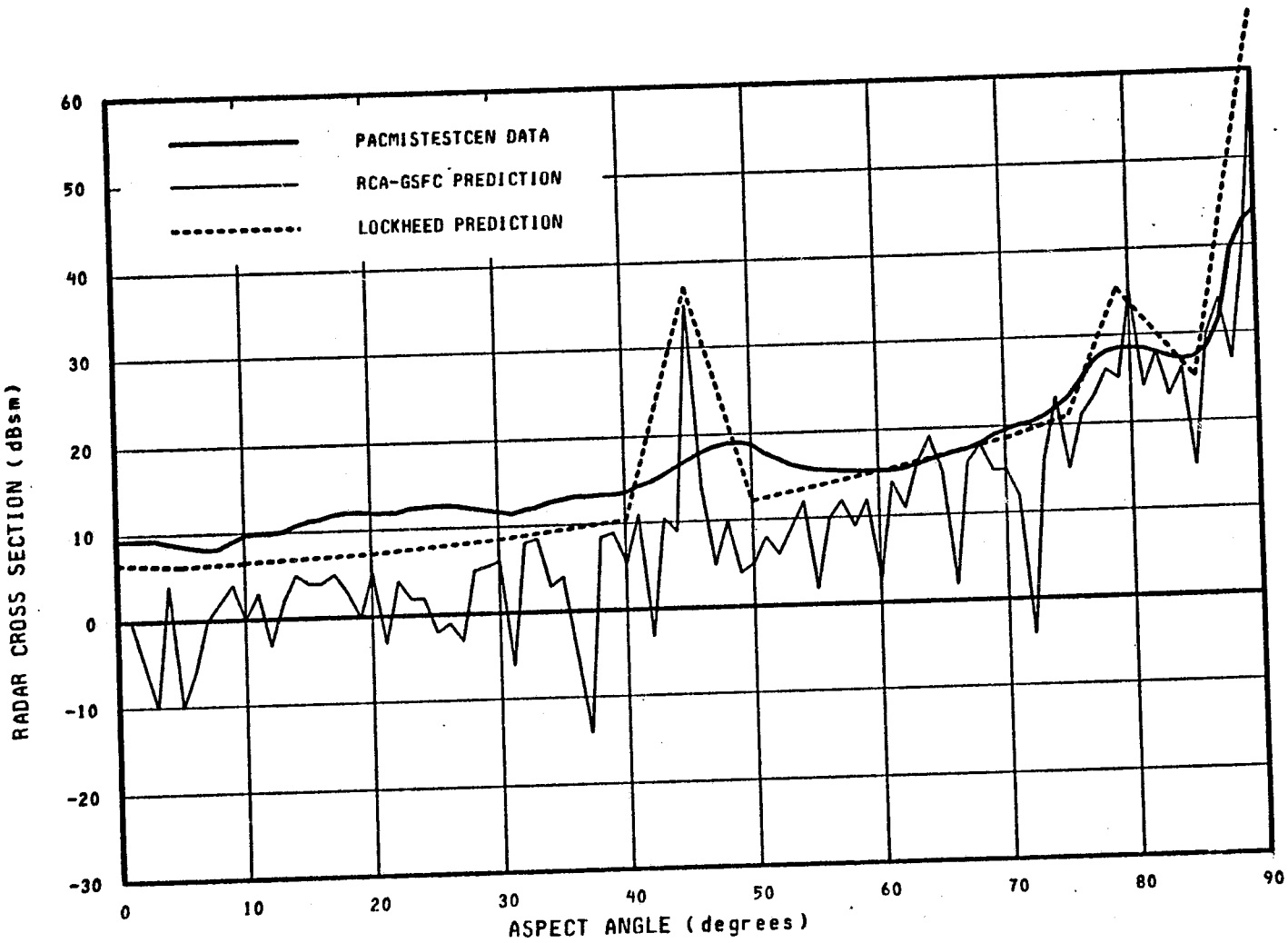

Figure 13. Measured and Predicted Radar Cross Section Data for the Space Shuttle Orbiter in the Yaw Plane.

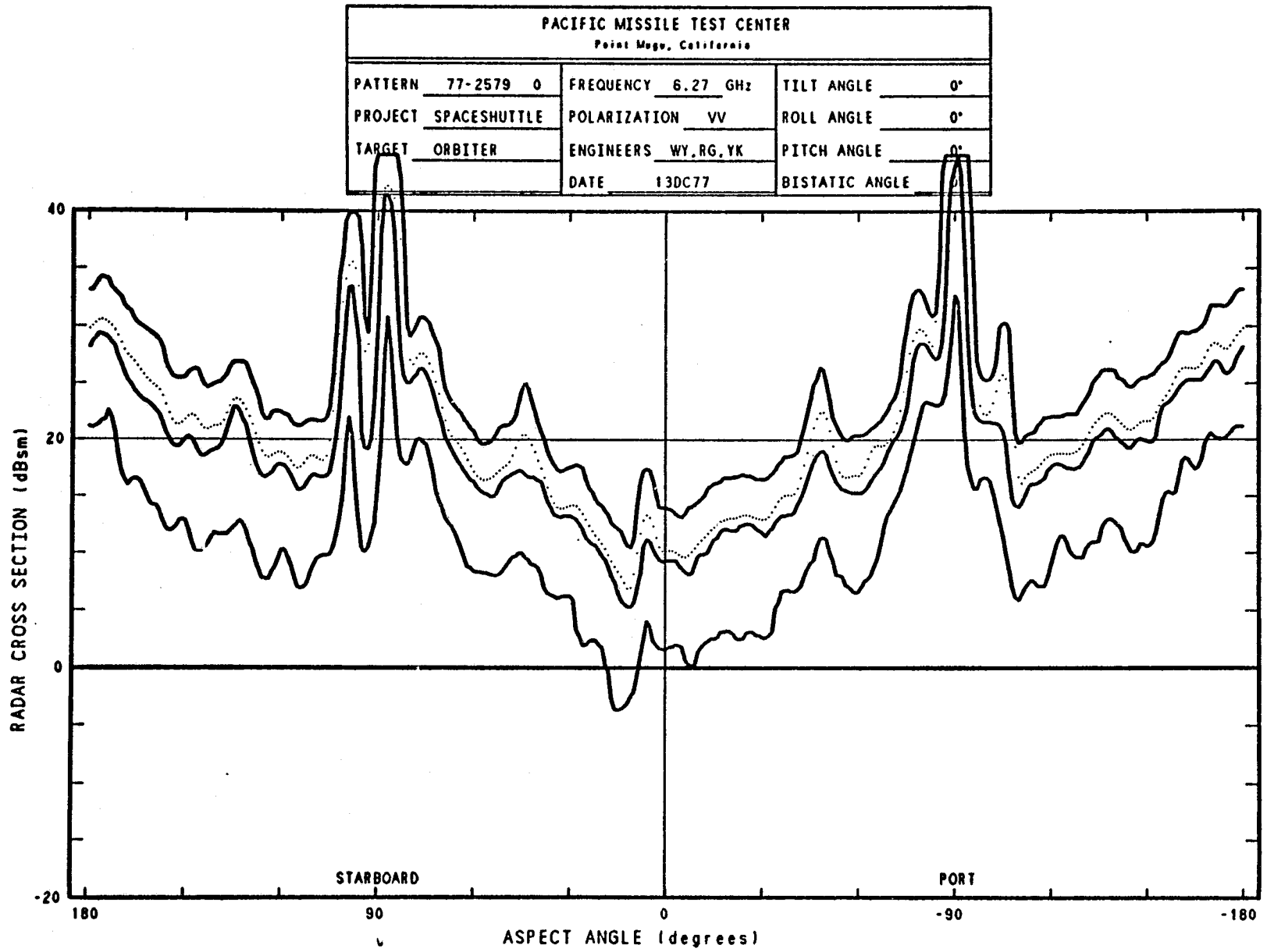

Figure 14. 10th, 50th, and 90th Percentiles and Mean of Radar Cross Section of Space Shuttle Orbiter, 0 Degrees Tilt Angle, 0 Degrees Roll Angle.

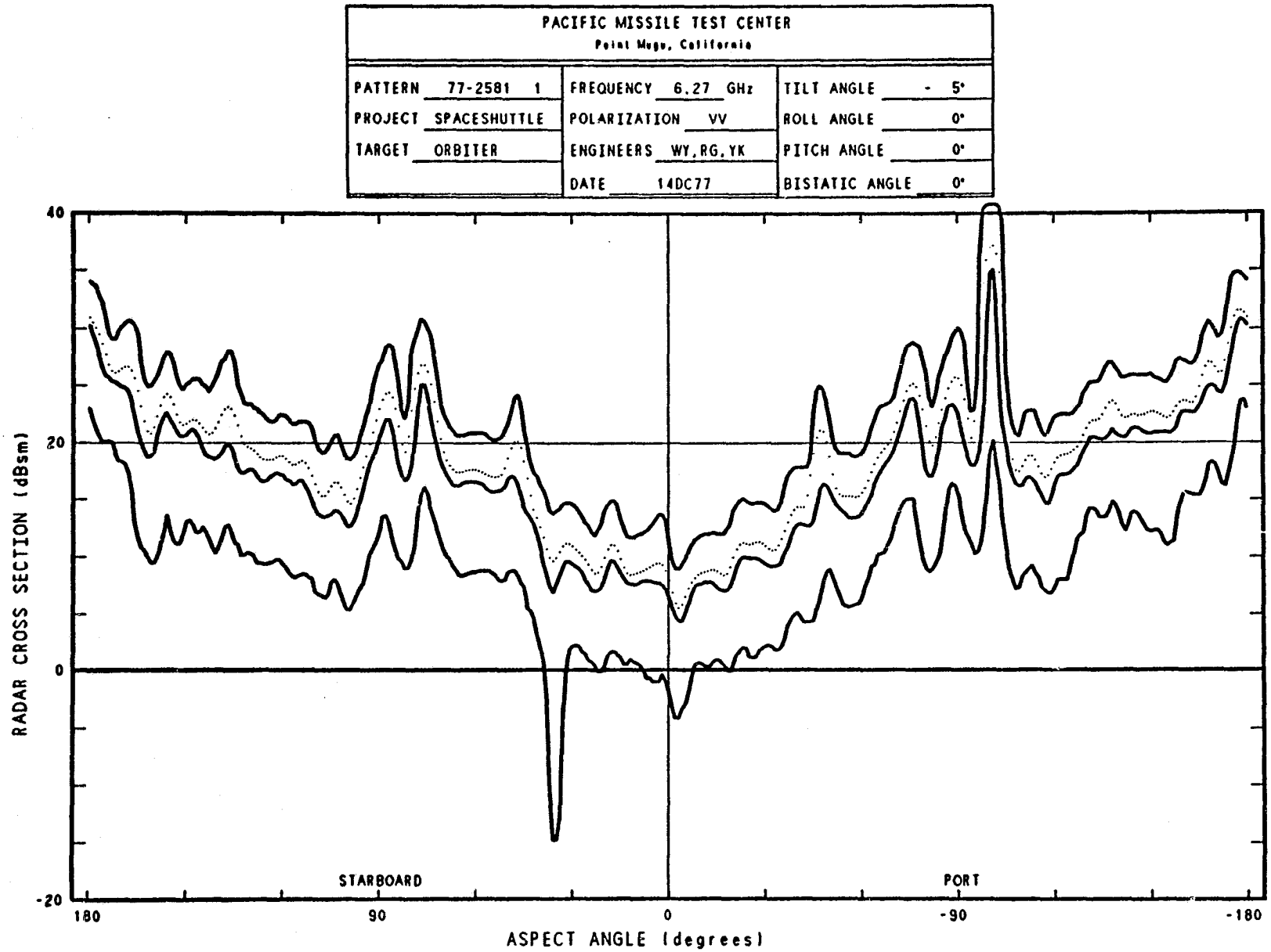

Figure 15. 10th, 50th, and 90th Percentiles and Mean of Radar Cross Section of Space Shuttle Orbiter, -5 Degrees Tilt Angle.

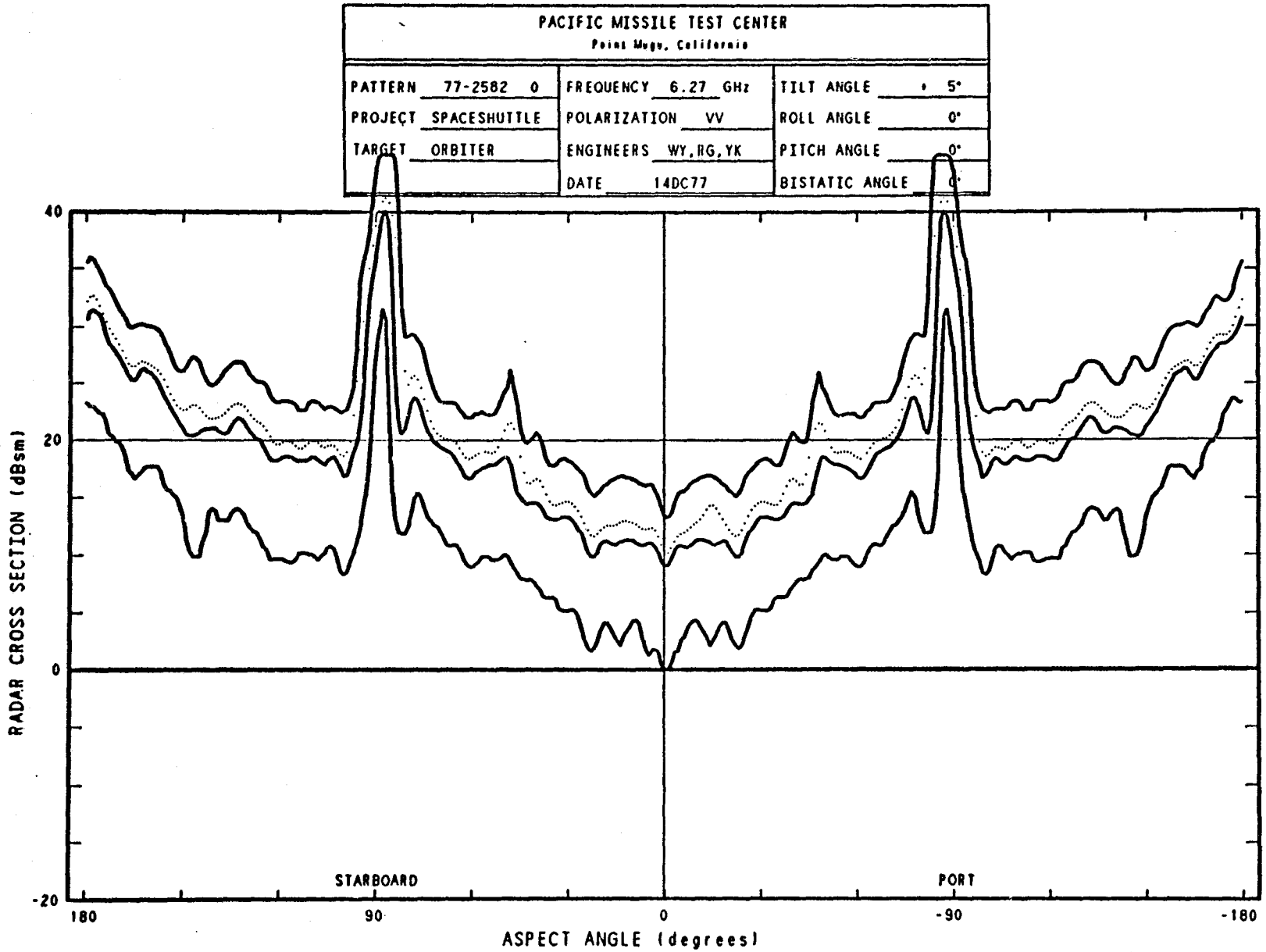

Figure 16. 10th, 50th, and 90th Percentiles and Mean of Radar Cross Section of Space Shuttle Orbiter, +5 Degrees Tilt Angle.

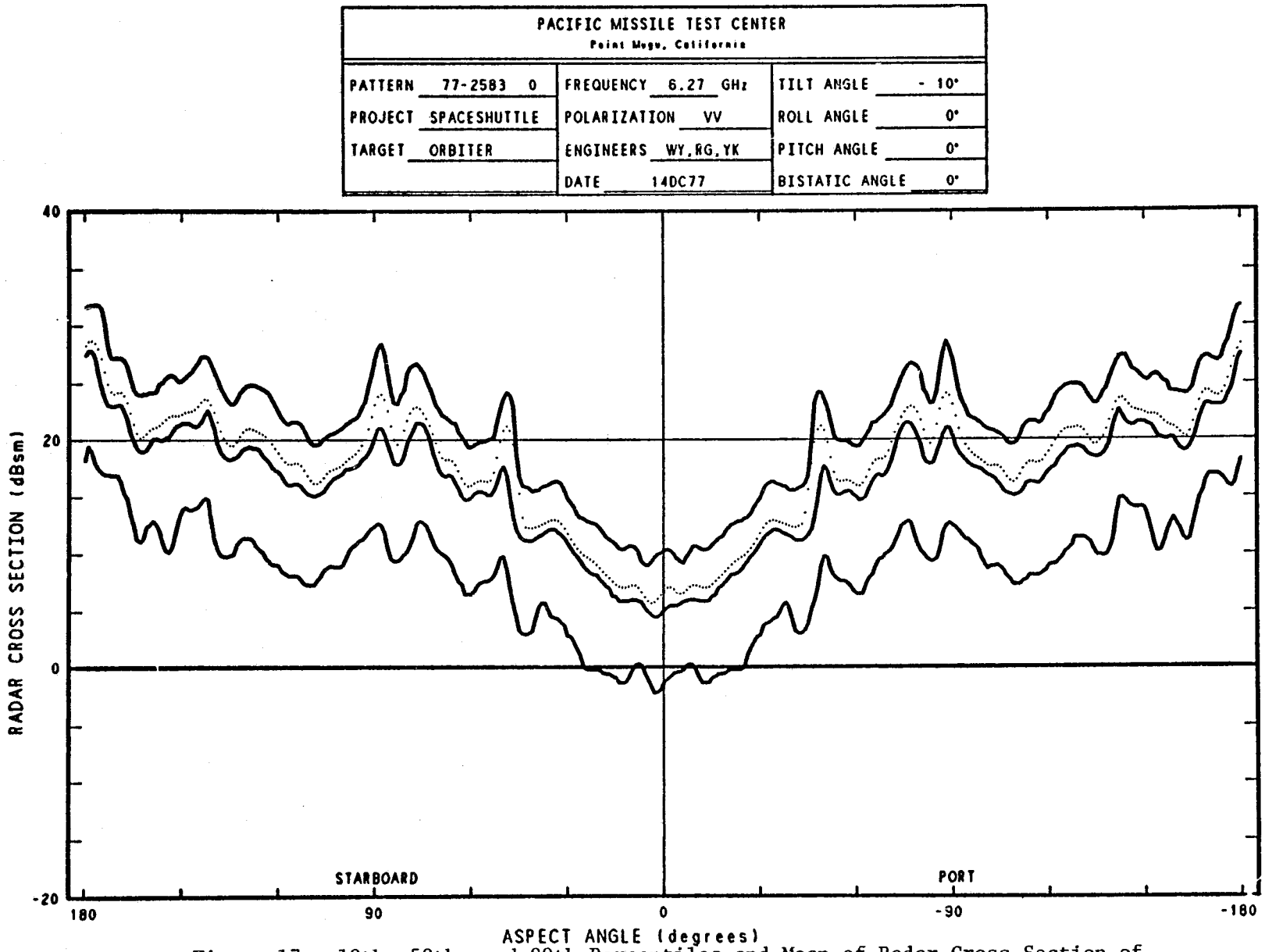

Figure 17. 10th, 50th, and 90th Percentiles and Mean of Radar Cross Section of Space Shuttle Orbiter, -10 Degrees Tilt Angle.

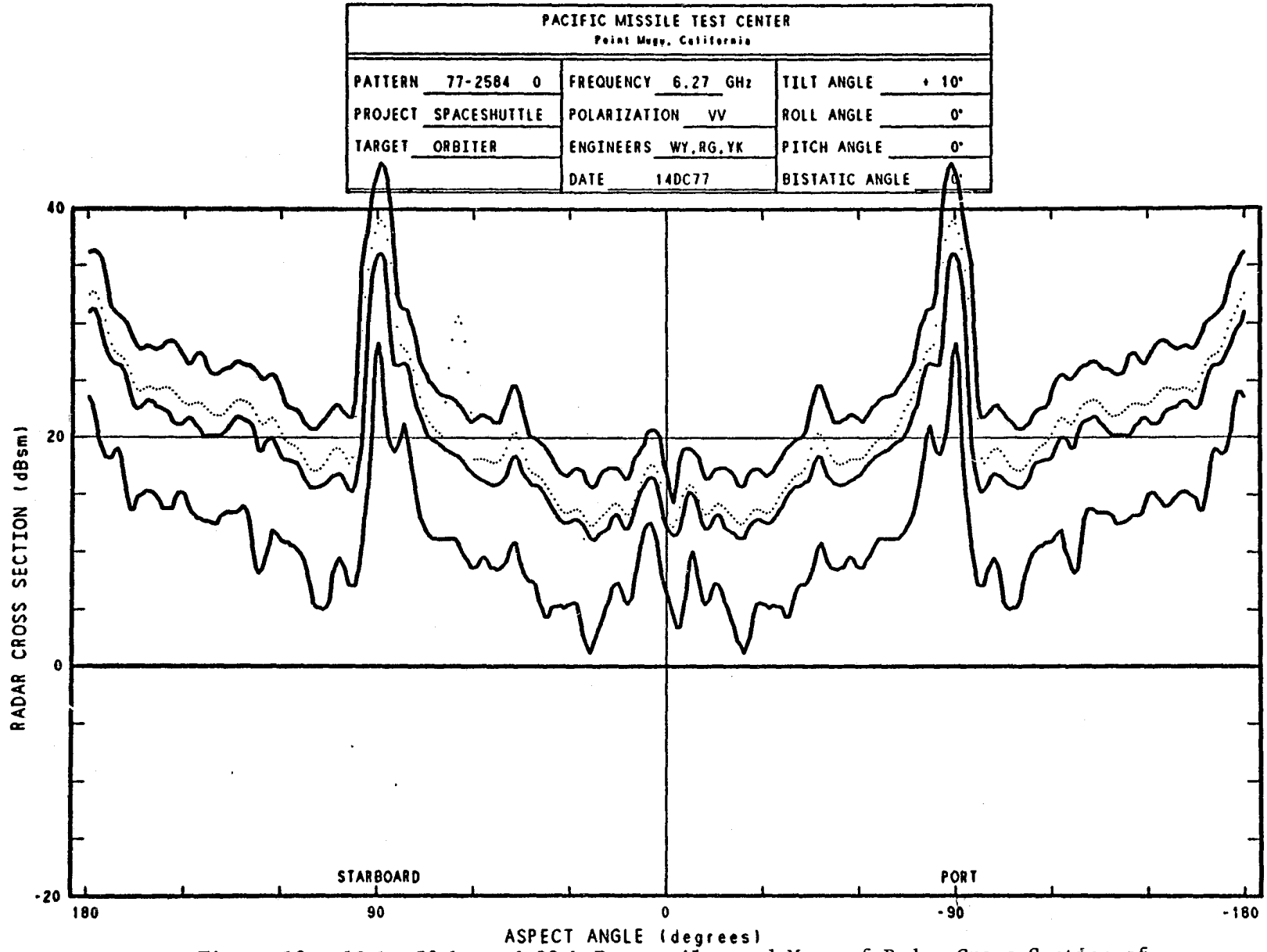

Figure 18. 10th, 50th, and 90th Percentiles and Mean of Radar Cross Section of Space Shuttle Orbiter, +10 Degrees Tilt Angle.

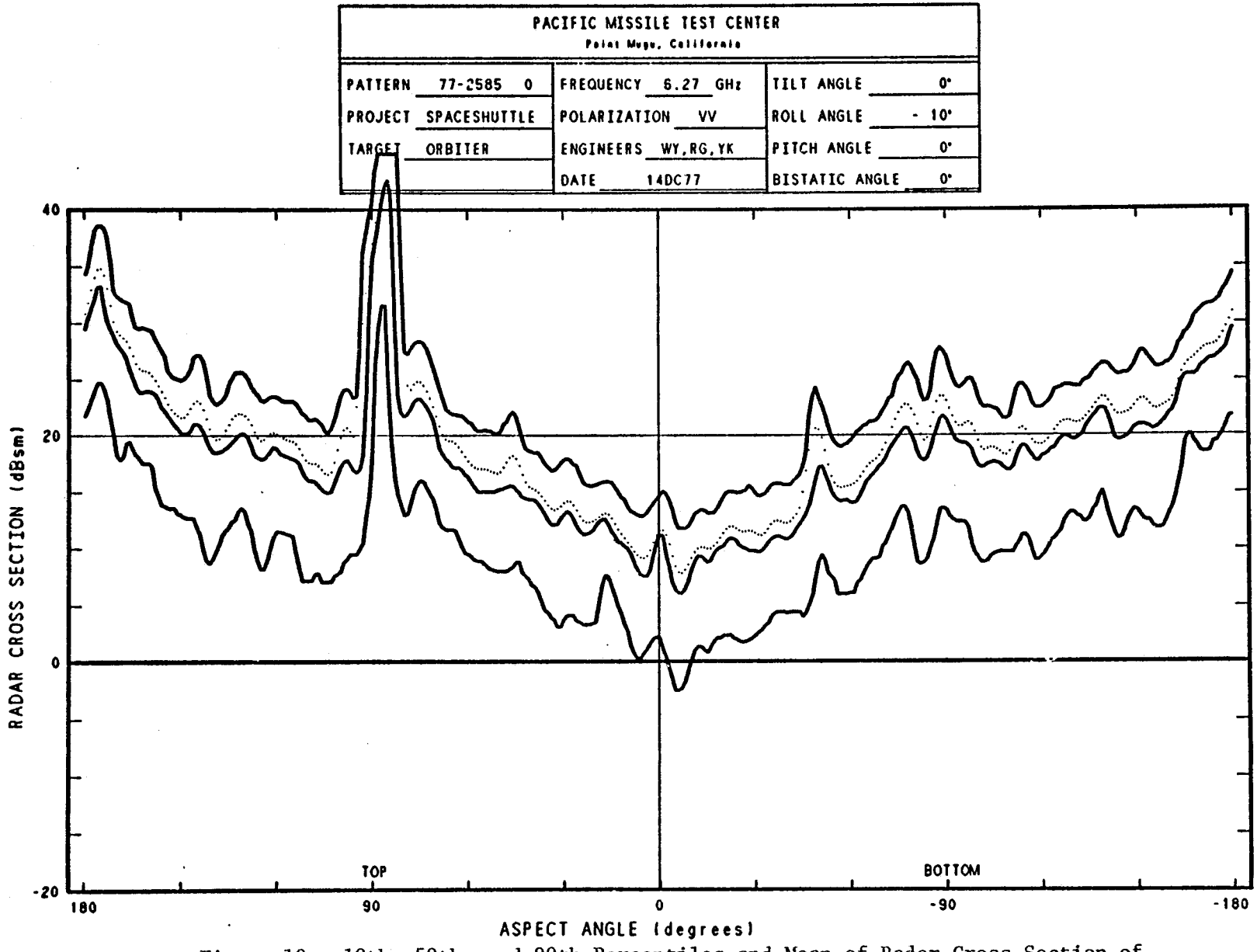

Figure 19. 10th, 50th, and 90th Percentiles and Mean of Radar Cross Section of Space Shuttle Orbiter, -10 Degrees Roll Angle.

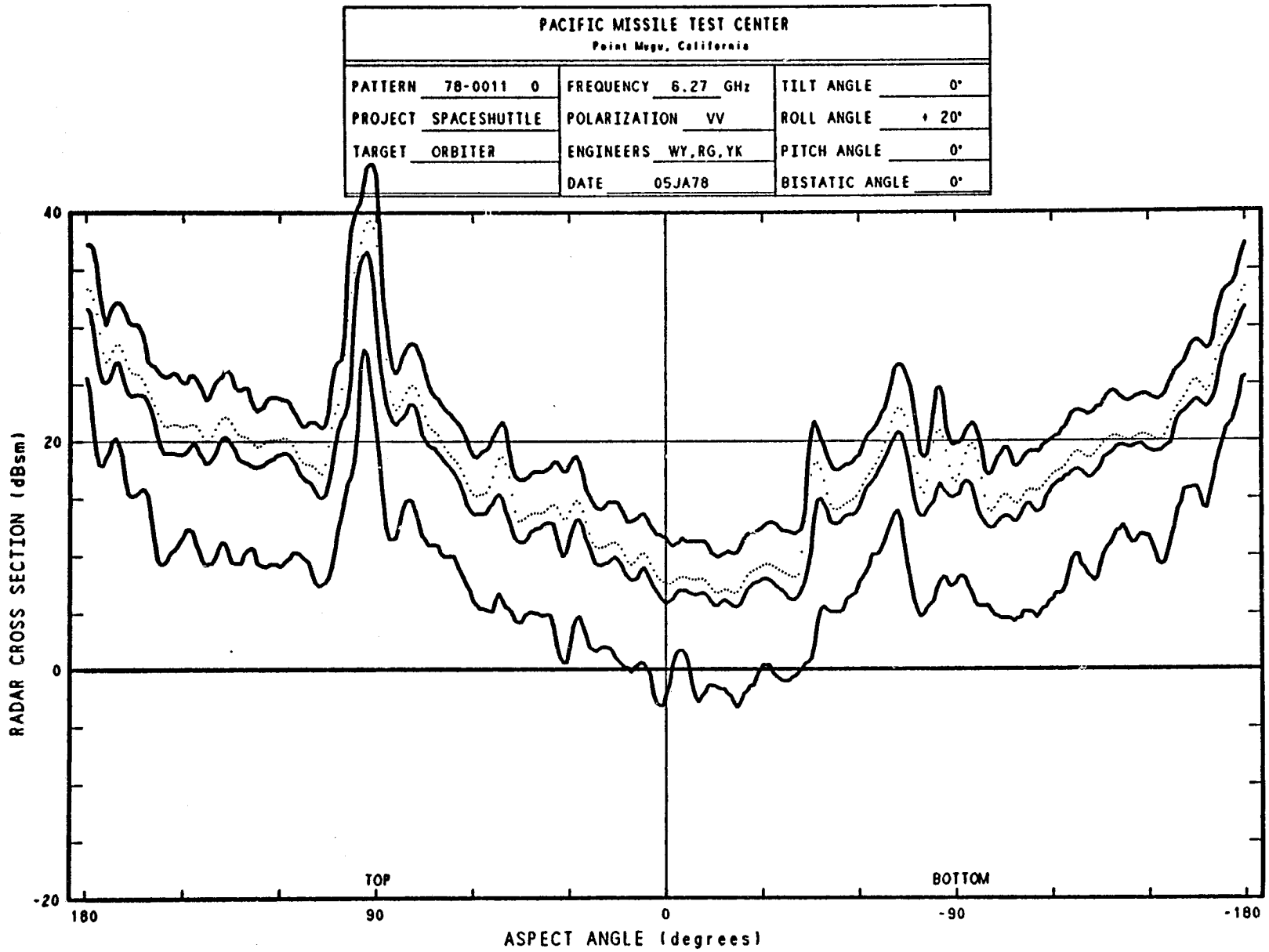

Figure 20. 10th, 50th, and 90th Percentiles and Mean of Radar Cross Section of Space Shuttle Orbiter, +20 Degrees Roll Angle.

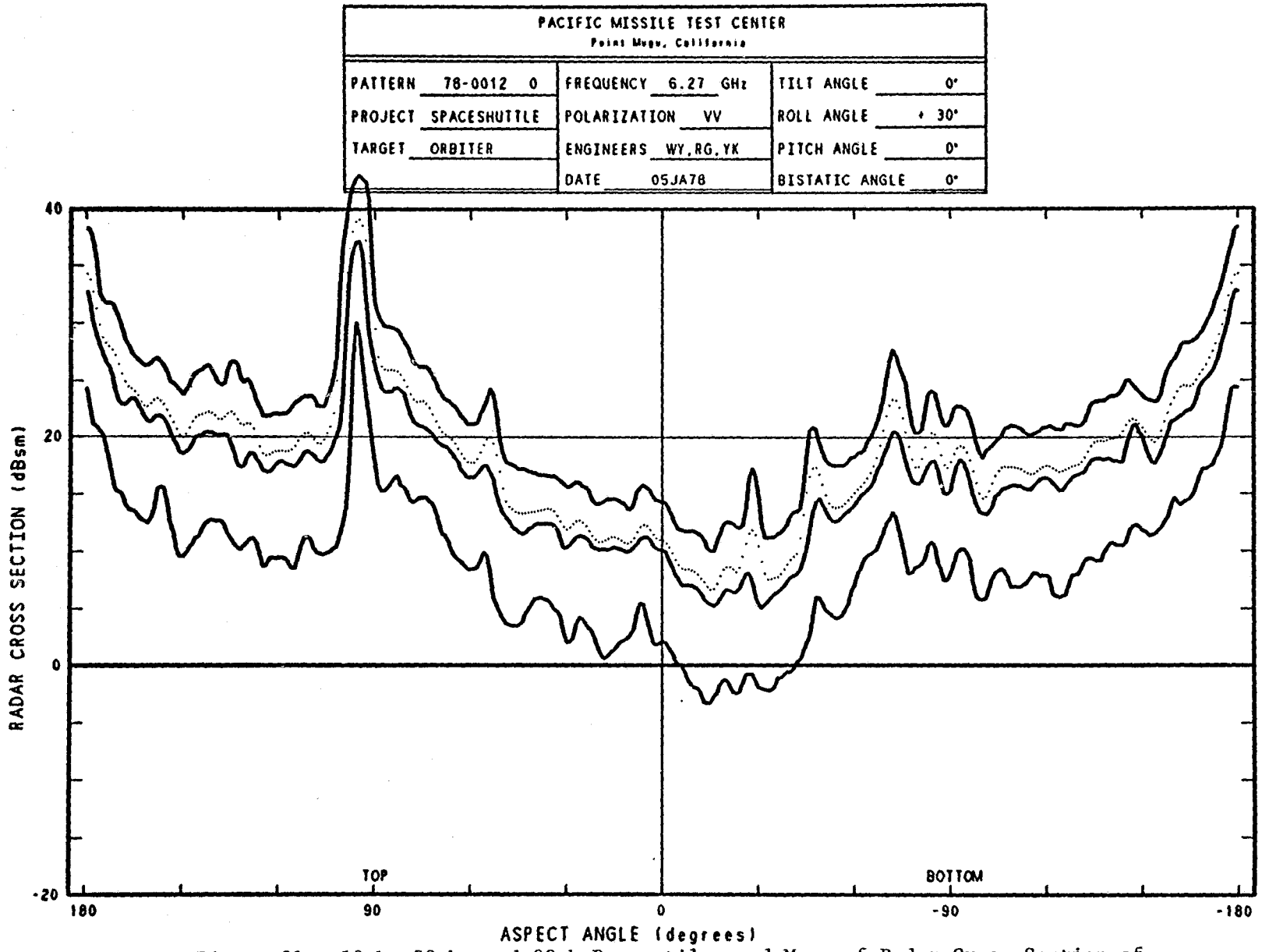

Figure 21. 10th, 50th, and 90th Percentiles and Mean of Radar Cross Section of Space Shuttle Orbiter, +30 Degrees Roll Angle.

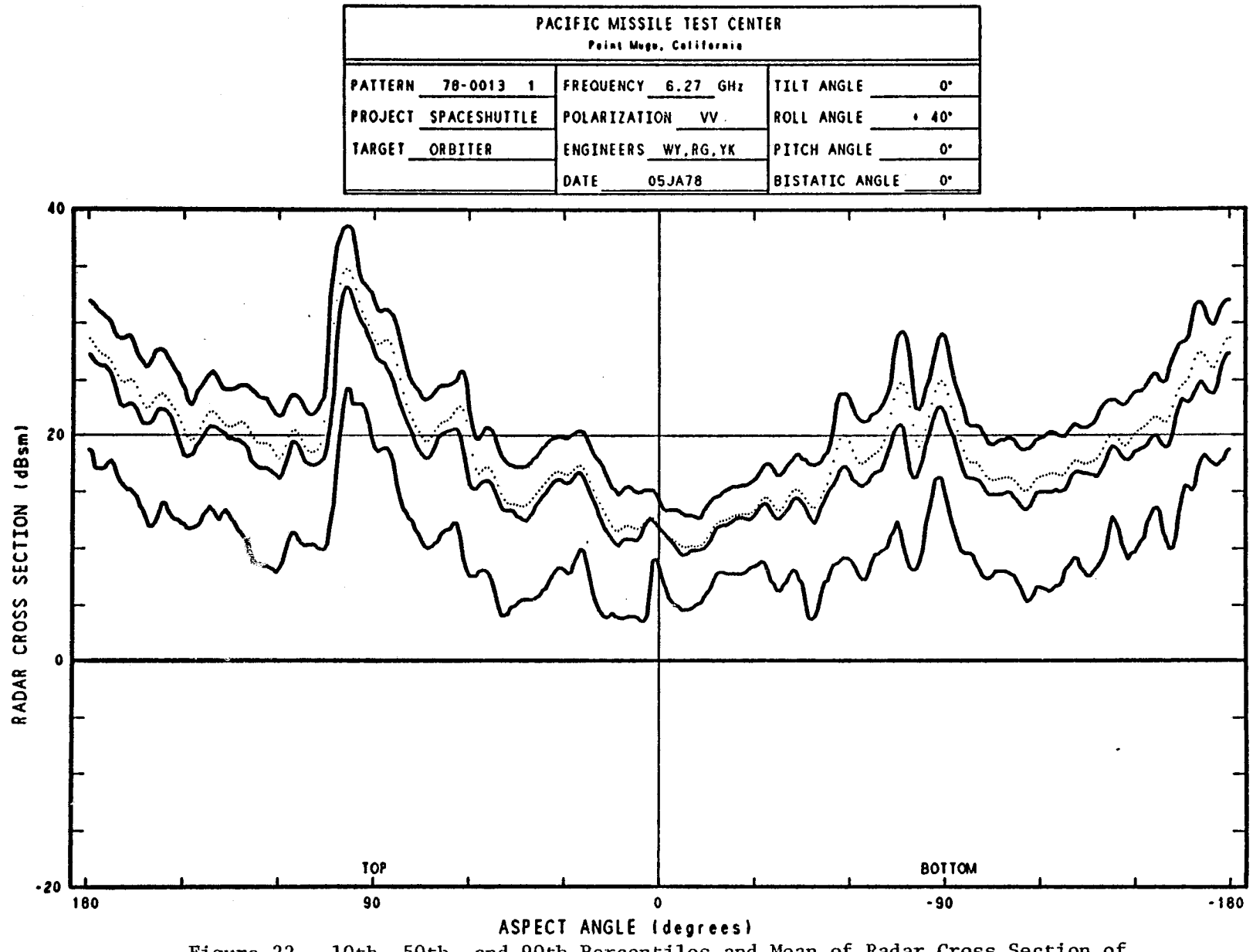

Figure 22. 10th, 50th, and 90th Percentiles and Mean of Radar Cross Section of Space Shuttle Orbiter, +40 Degrees Roll Angle.

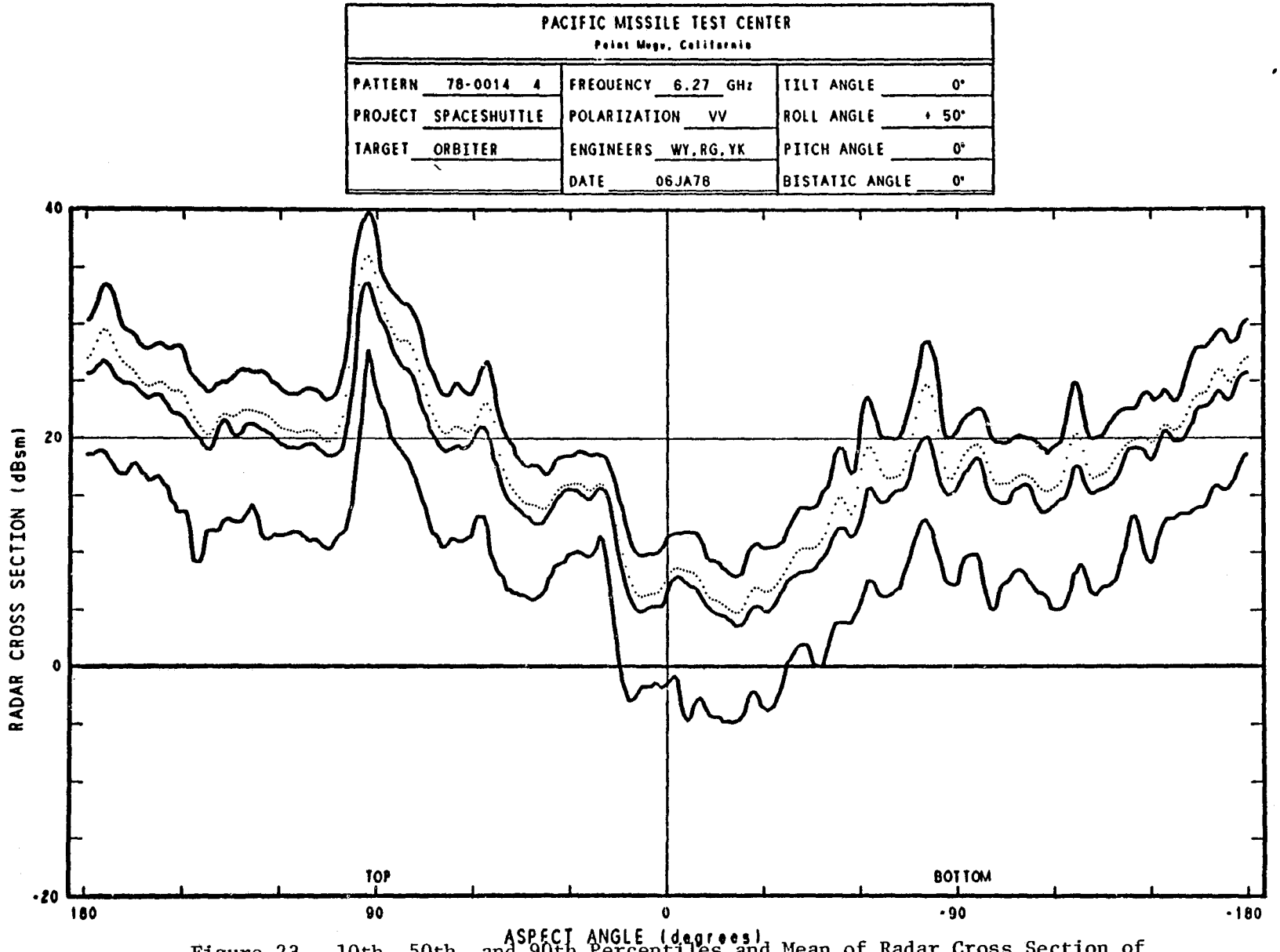

Figure 23. 10th, 50th, and 90th Percentiles and Mean of Radar Cross Section of Space Shuttle Orbiter, +50 Degrees Roll Angle.

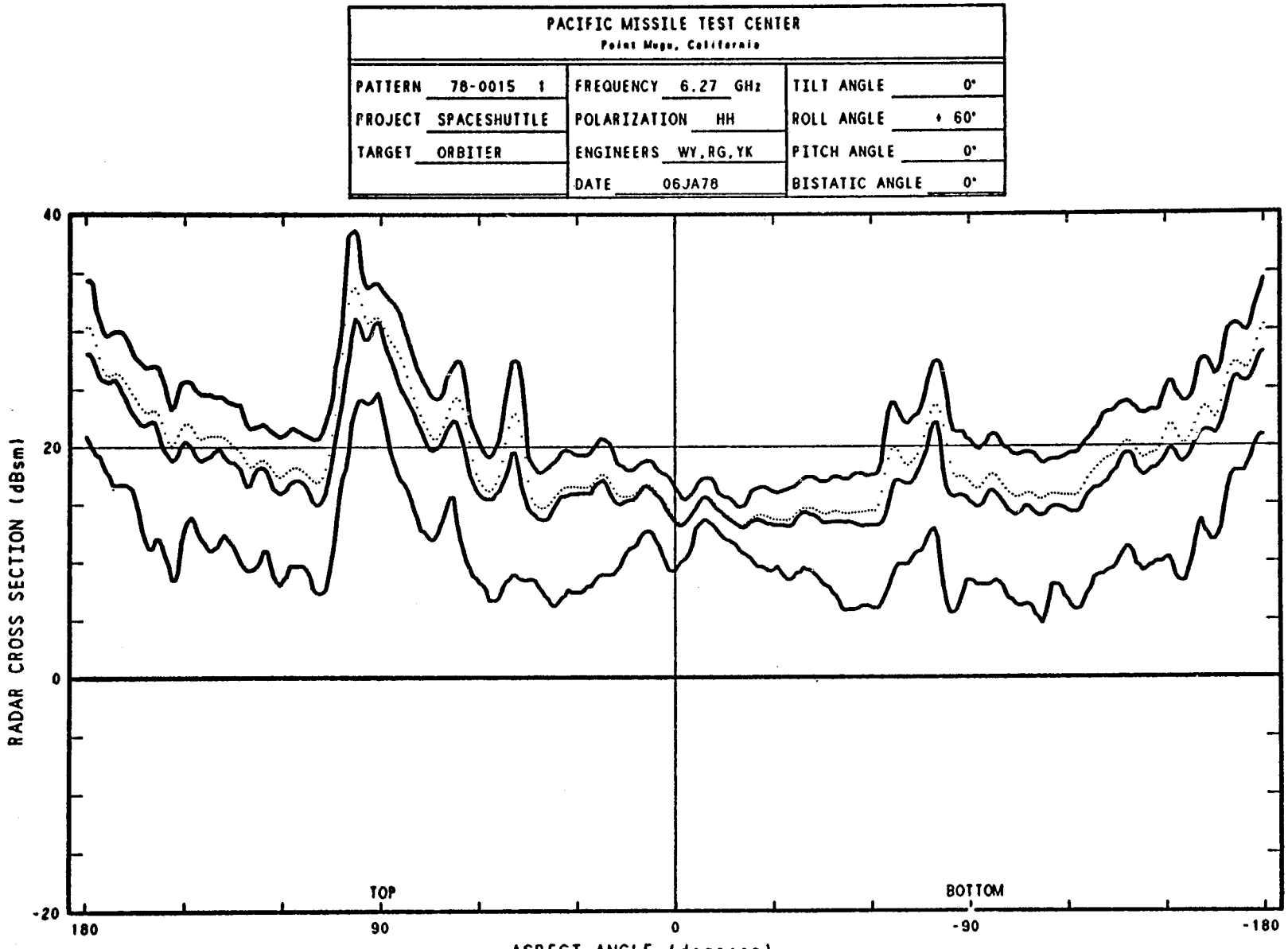

Figure 24. 10th, 50th, and 90th Percentiles and Mean of Radar Cross Section of Space Shuttle Orbiter, +60 Degrees Roll Angle.

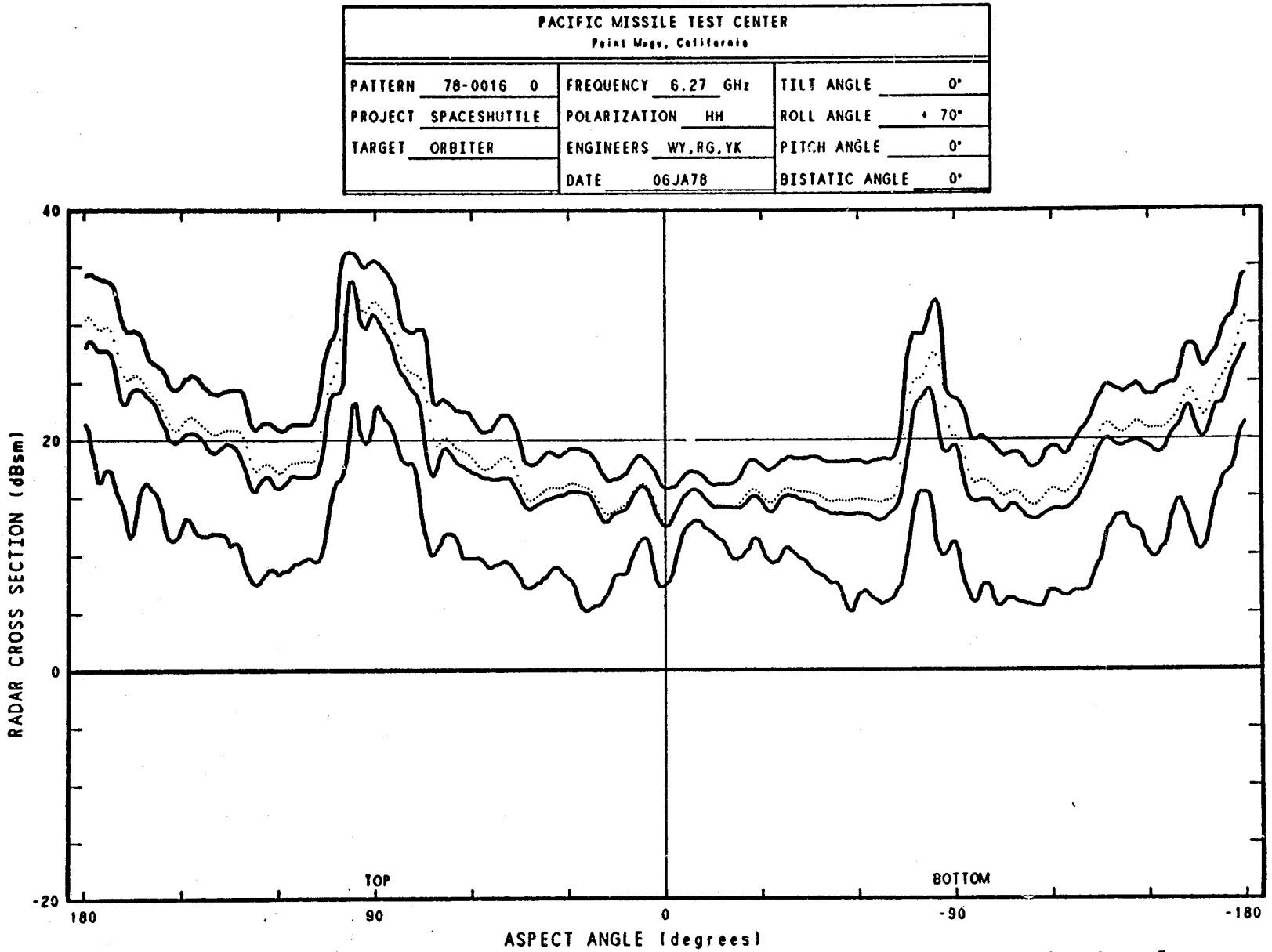

Figure 25. 10th, 50th, and 90th Percentiles and Mean of Radar Cross Section of Space Shuttle Orbiter, +70 Degrees Roll Angle.

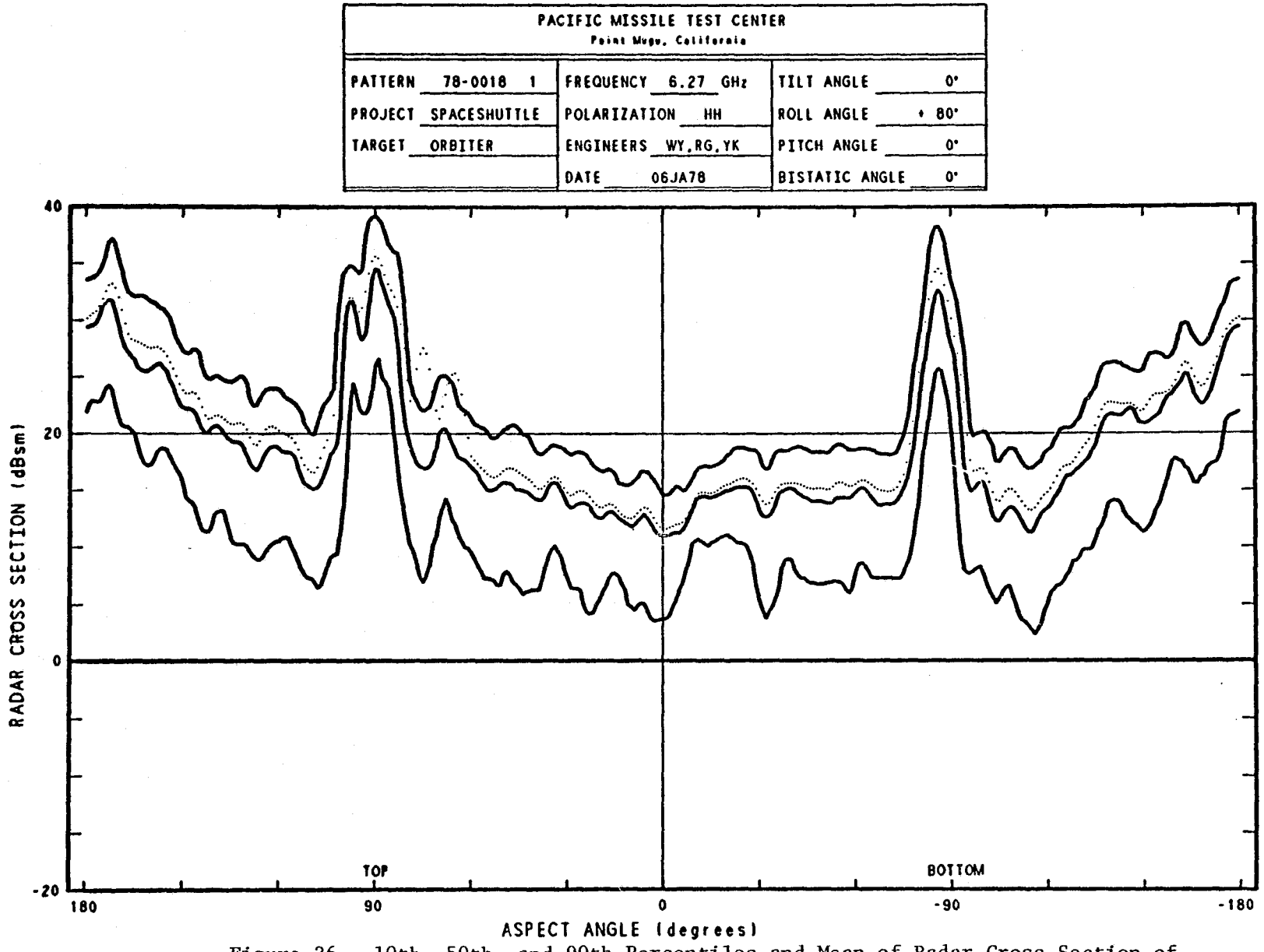

Figure 26. 10th, 50th, and 90th Percentiles and Mean of Radar Cross Section of Space Shuttle Orbiter, +80 Degrees Roll Angle.

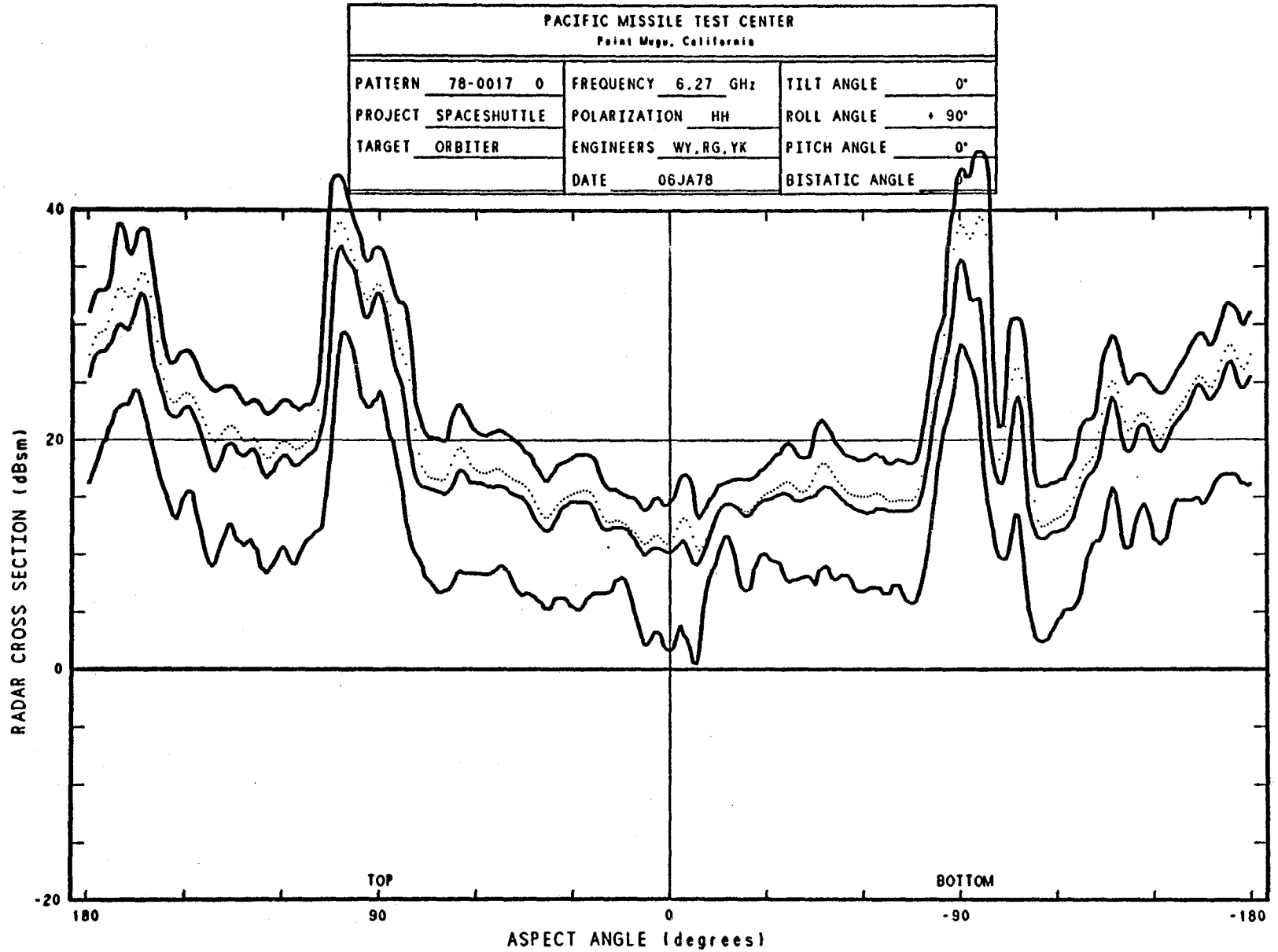

Figure 27. 10th, 50th, and 90th Percentiles and Mean of Radar Cross Section of Space Shuttle Orbiter, +90 Degrees Roll Angle.

PACIFIC MISSILE TEST CENTER Point Mugu, California		
PATTERN 77-2579 00	FREQUENCY 6.27 GHz	TILT ANGLE 0°
PROJECT SPACESHUTTLE	POLARIZATION VV	ROLL ANGLE 0°
TARGET ORBITER	ENGINEERS WY,RG,YK	PITCH ANGLE 0°
	DATE 13DC77	BISTATIC ANGLE 0°

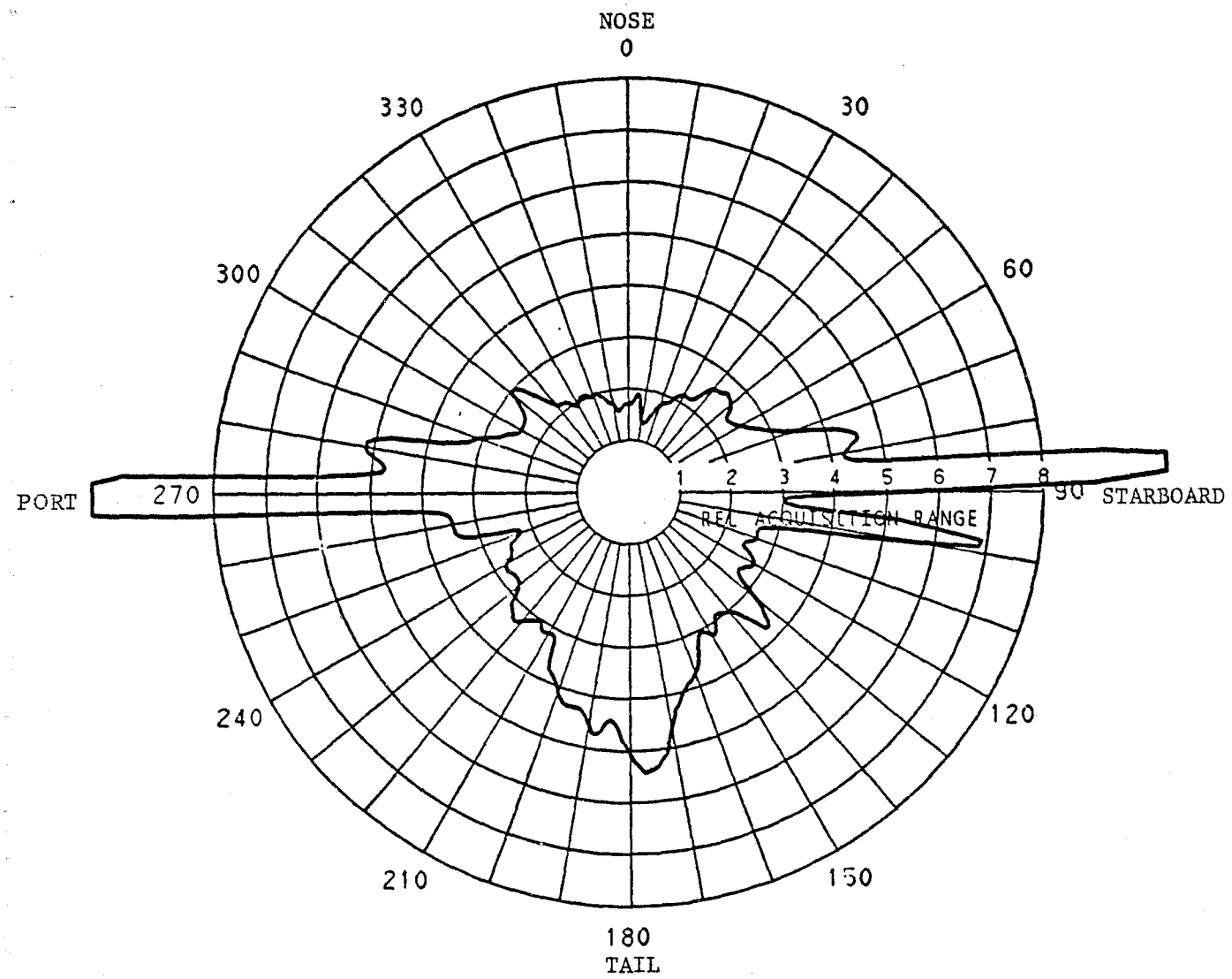

Figure 28. Fourth Root of Median Radar Cross Section of Space Shuttle Orbiter, 0 Degrees Tilt Angle, 0 Degrees Roll Angle.

PACIFIC MISSILE TEST CENTER Point Mugu, California		
PATTERN 77-2581 00	FREQUENCY 6.27 GHz	TILT ANGLE - 5°
PROJECT SPACESHUTTLE	POLARIZATION VV	ROLL ANGLE 0°
TARGET ORBITER	ENGINEERS WY,RG,YK	PITCH ANGLE 0°
	DATE 14DC77	BISTATIC ANGLE 0°

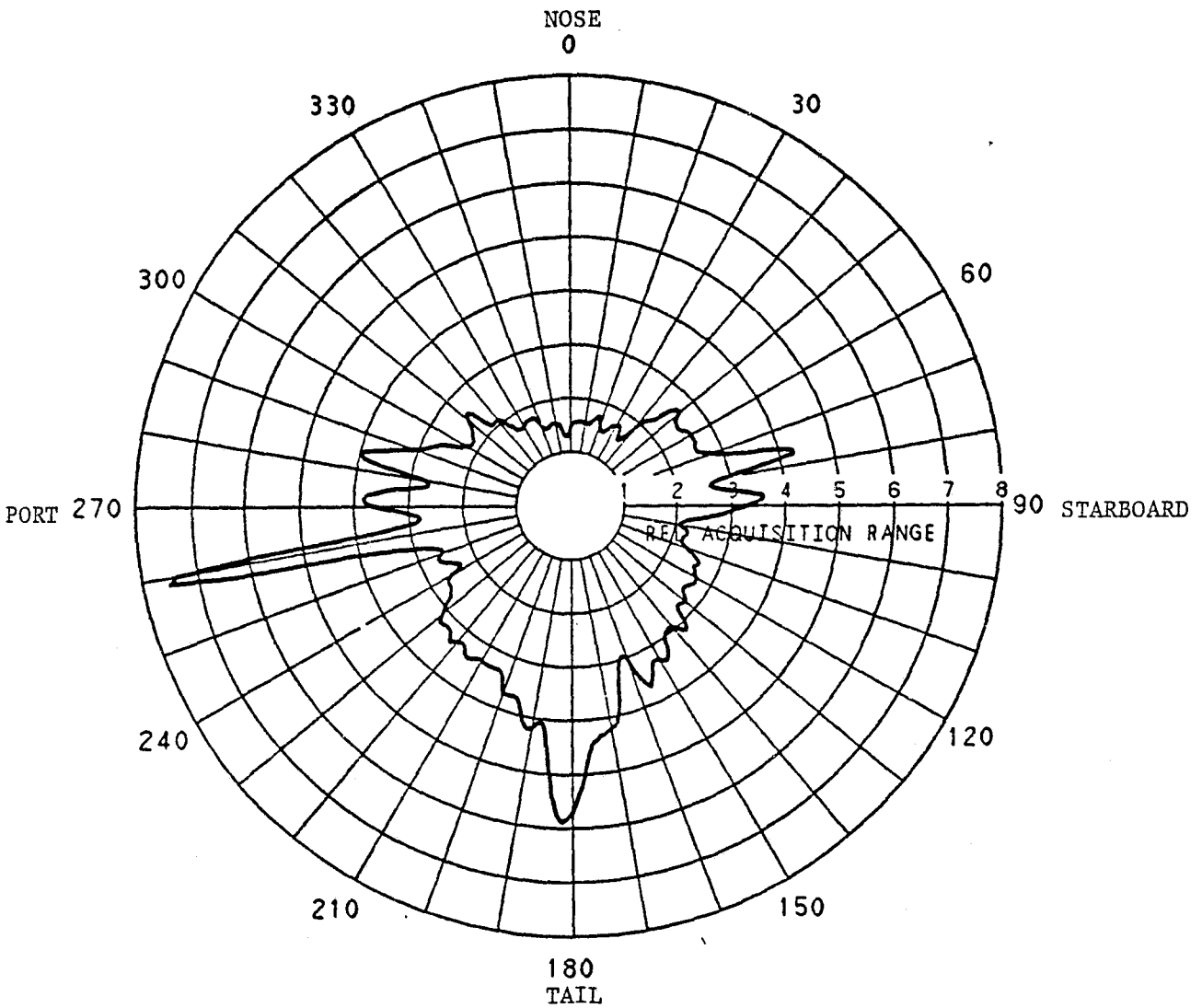

Figure 29. Fourth Root of Median Radar Cross Section of Space Shuttle Orbiter, -5 Degrees Tilt Angle.

PACIFIC MISSILE TEST CENTER Point Mugu, California		
PATTERN 77-2582 00	FREQUENCY 6.27 GHz	TILT ANGLE + 5°
PROJECT SPACESHUTTLE	POLARIZATION VV	ROLL ANGLE 0°
TARGET ORBITER	ENGINEERS WY,RG,YK	PITCH ANGLE 0°
	DATE 14DC77	BISTATIC ANGLE 0°

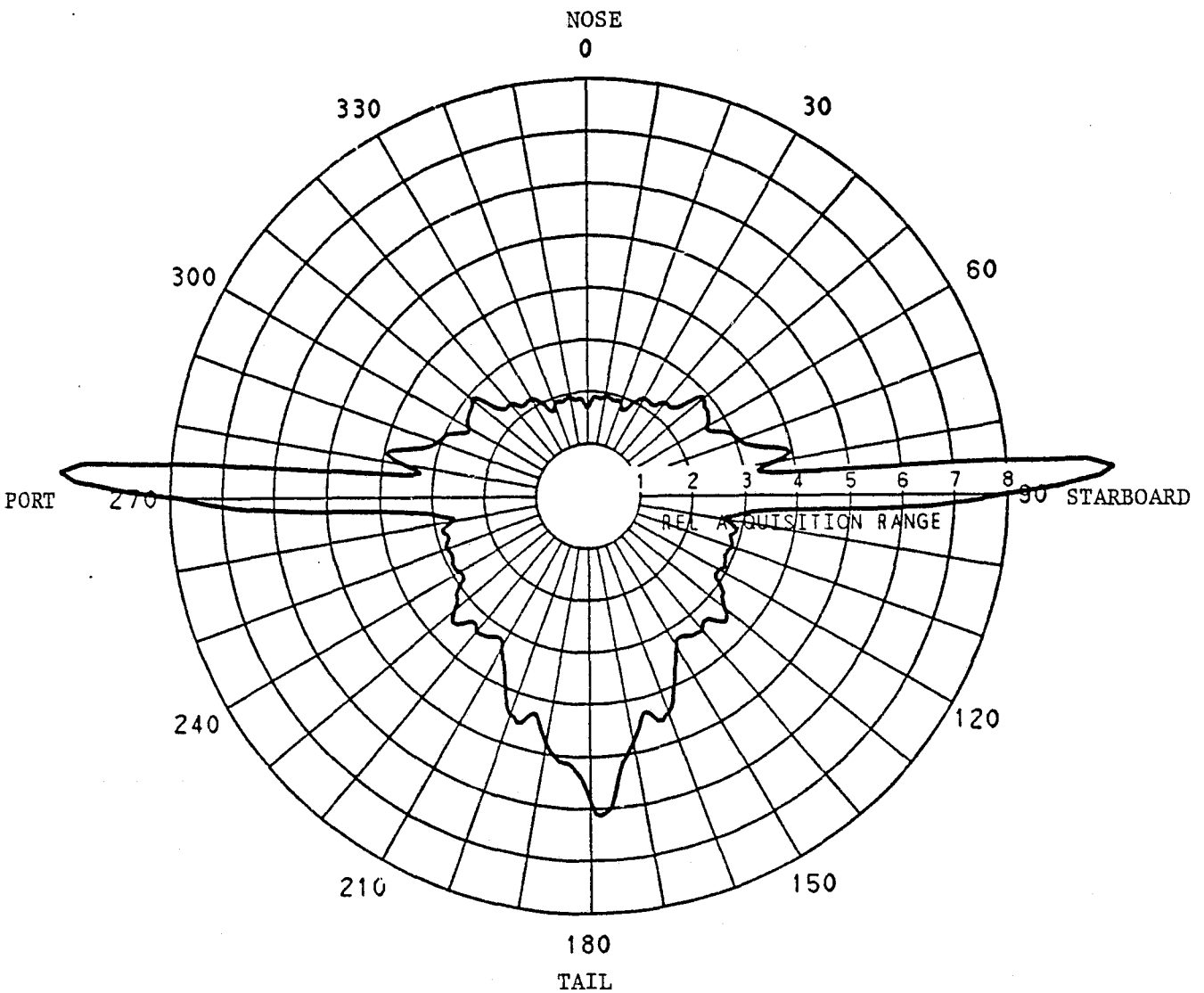

Figure 30. Fourth Root of Median Radar Cross Section of Space Shuttle Orbiter, +5 Degrees Tilt Angle.

PACIFIC MISSILE TEST CENTER Point Mugu, California		
PATTERN 77-2583 00	FREQUENCY 6.27 GHz	TILT ANGLE - 10°
PROJECT SPACESHUTTLE	POLARIZATION VV	ROLL ANGLE 0°
TARGET ORBITER	ENGINEERS WY,RG,YK	PITCH ANGLE 0°
	DATE 14DC77	BISTATIC ANGLE 0°

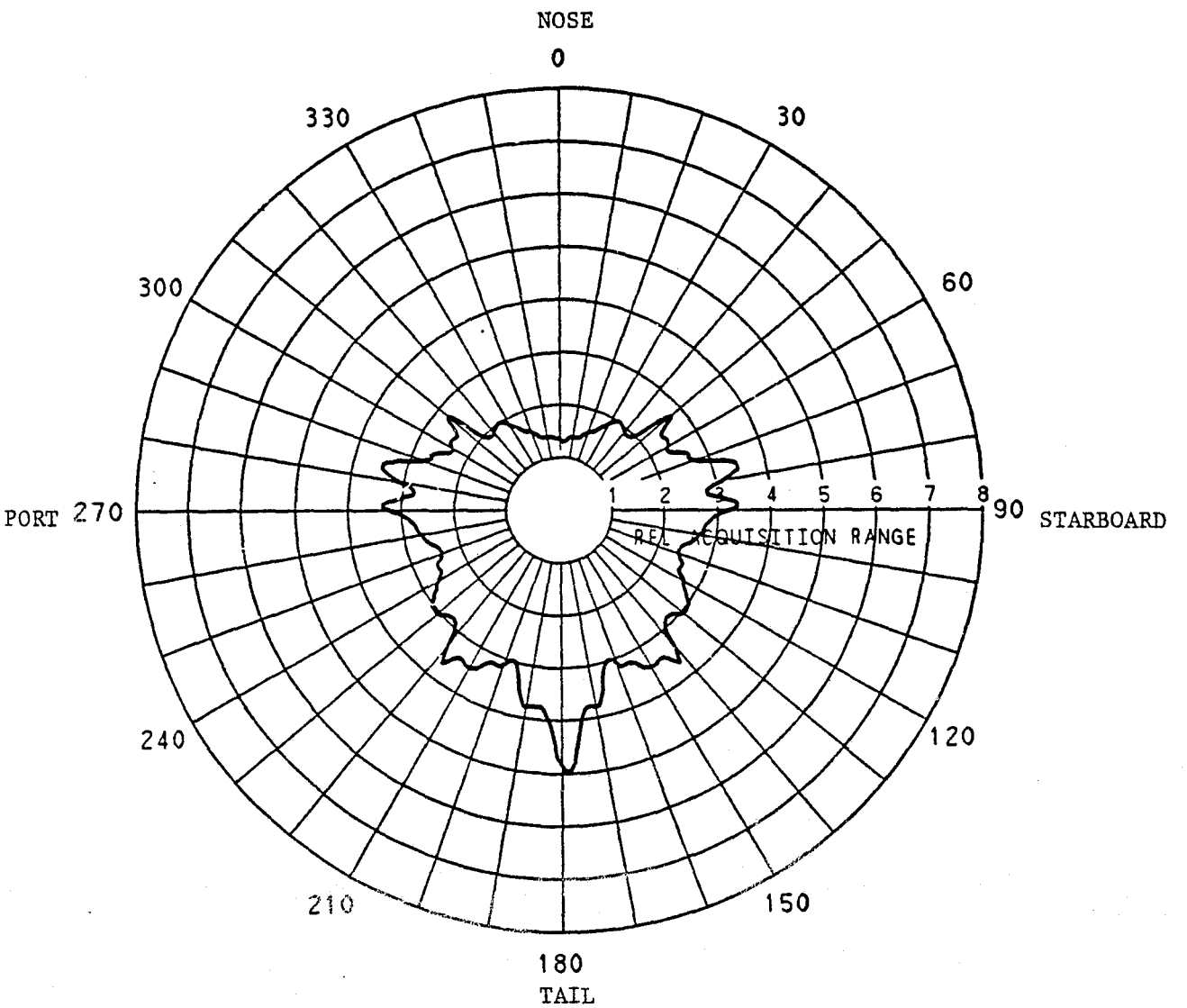

Figure 31. Fourth Root of Median Radar Cross Section of Space Shuttle Orbiter, -10 Degrees Tilt Angle.

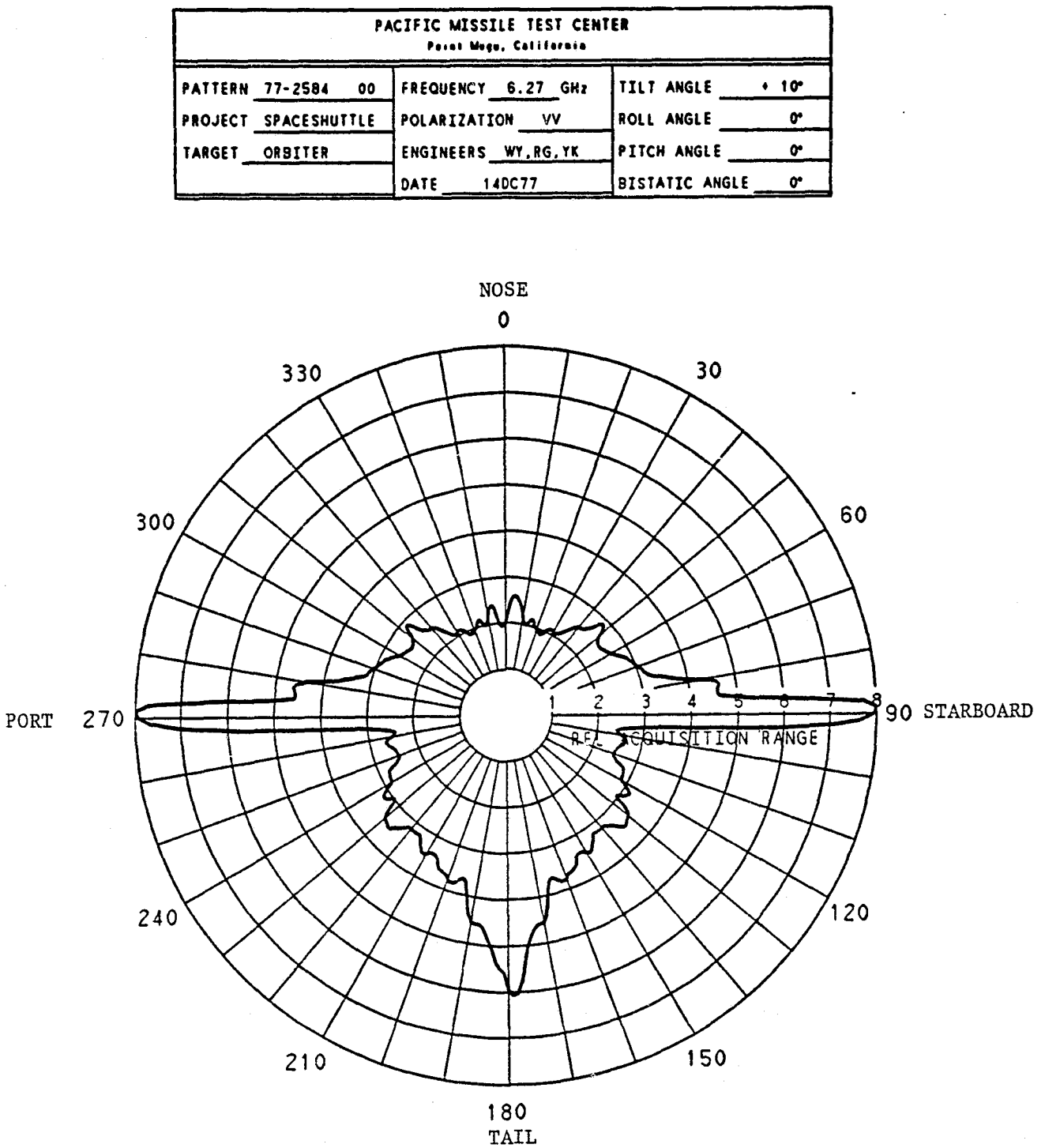

Figure 32. Fourth Root of Median Radar Cross Section of Space Shuttle Orbiter, +10 Degrees Tilt Angle.

PACIFIC MISSILE TEST CENTER Point Mugu, California		
PATTERN 77-2585 00	FREQUENCY 6.27 GHz	TILT ANGLE 0°
PROJECT SPACESHUTTLE	POLARIZATION VV	ROLL ANGLE - 10°
TARGET ORBITER	ENGINEERS WY,RG,YK	PITCH ANGLE 0°
	DATE 14DC77	BISTATIC ANGLE 0°

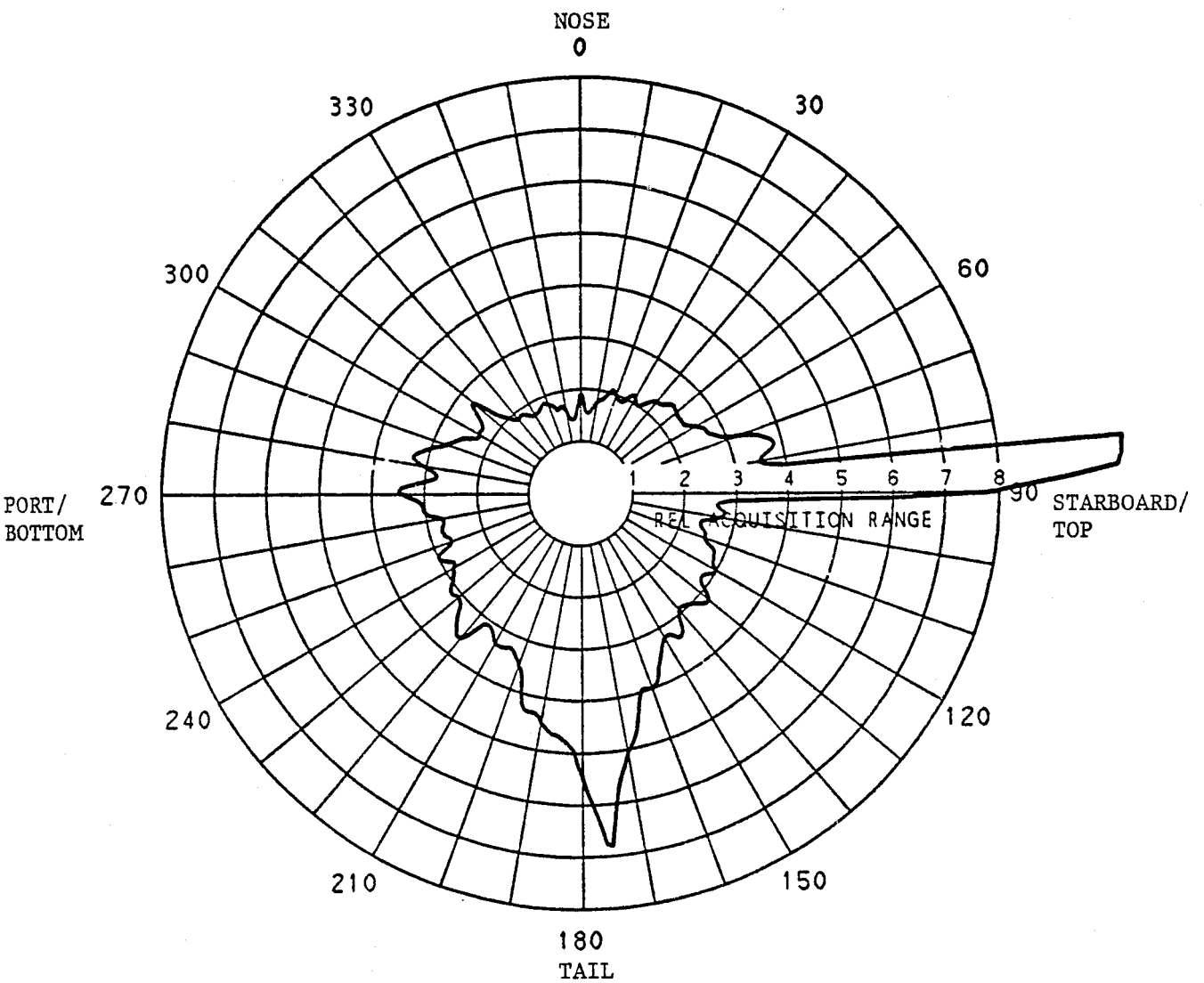

Figure 33. Fourth Root of Median Radar Cross Section of Space Shuttle Orbiter, -10 Degrees Roll Angle.

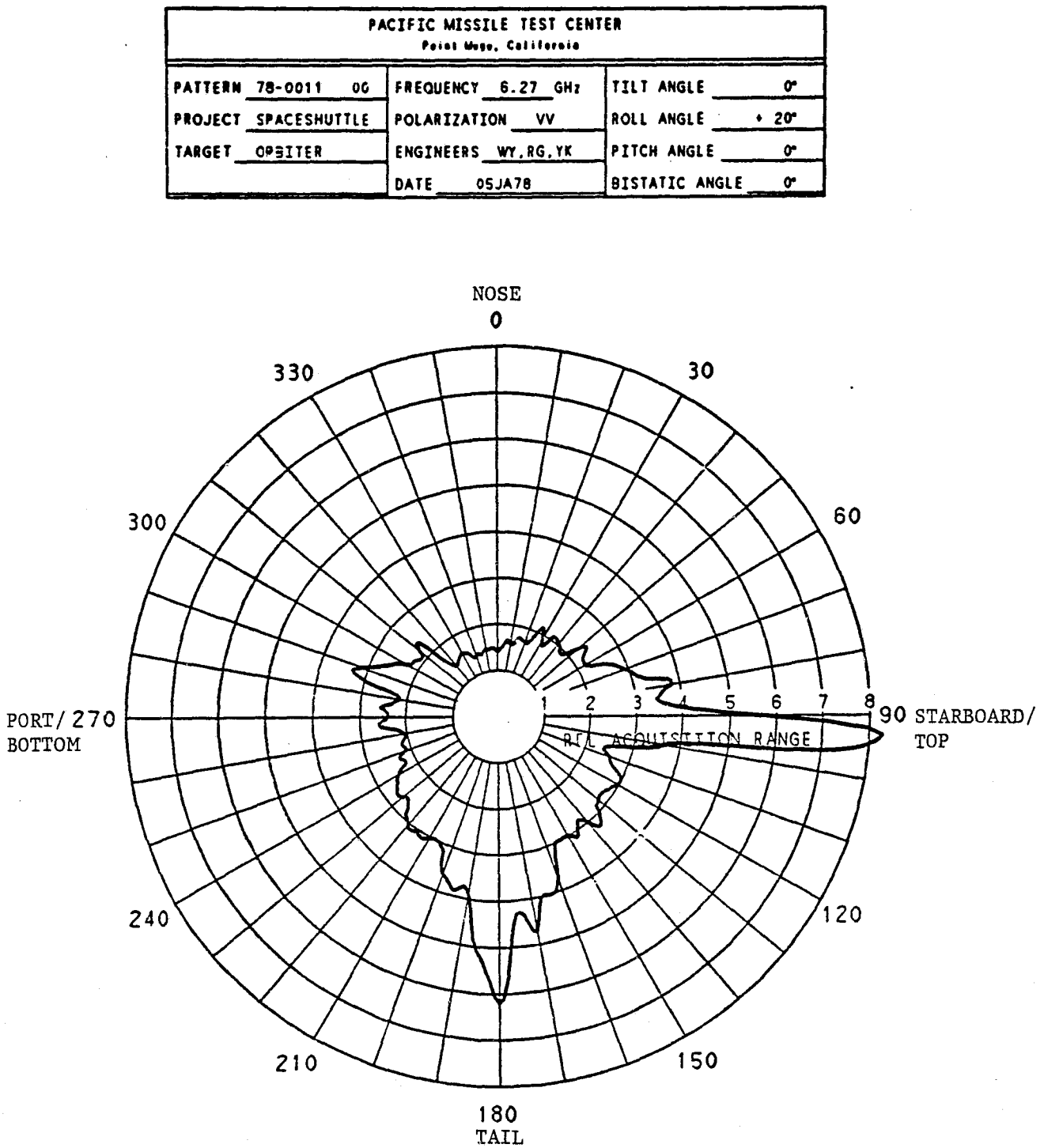

Figure 34. Fourth Root of Median Radar Cross Section of Space Shuttle Orbiter, +20 Degrees Roll Angle.

PACIFIC MISSILE TEST CENTER Point Mugu, California		
PATTERN 78-0012 00	FREQUENCY 6.27 GHz	TILT ANGLE 0°
PROJECT SPACESHUTTLE	POLARIZATION VV	ROLL ANGLE + 30°
TARGET ORBITER	ENGINEERS WY,RG,YK	PITCH ANGLE 0°
	DATE 05JA78	BISTATIC ANGLE 0°

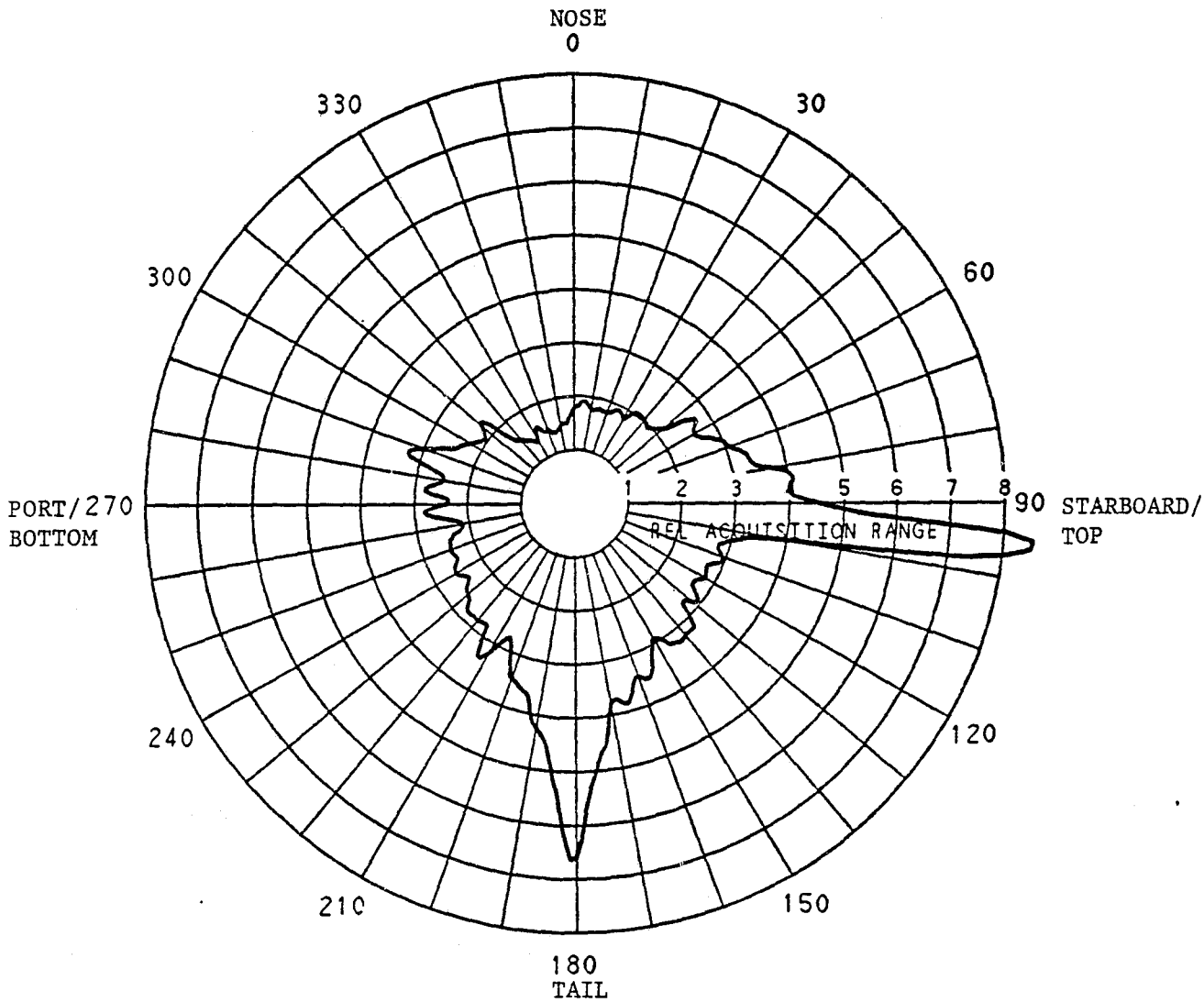

Figure 35. Fourth Root of Median Radar Cross Section of Space Shuttle Orbiter, +30 Degrees Roll Angle.

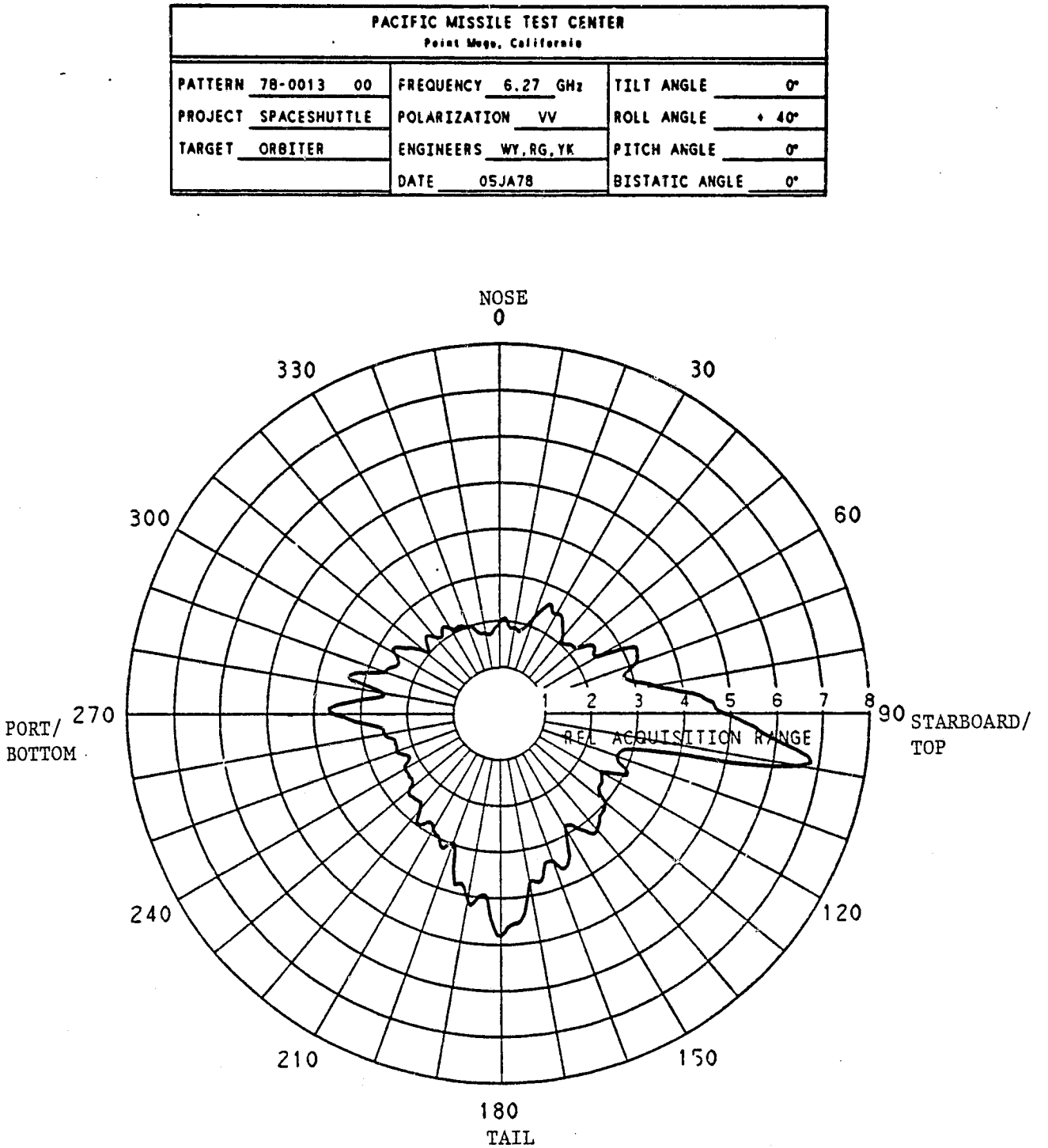

Figure 36. Fourth Root of Median Radar Cross Section of Space Shuttle Orbiter, +40 Degrees Roll Angle.

PACIFIC MISSILE TEST CENTER Point Mugu, California		
PATTERN 78-0014 00	FREQUENCY 6.27 GHz	TILT ANGLE 0°
PROJECT SPACESHUTTLE	POLARIZATION VV	ROLL ANGLE + 50°
TARGET ORBITER	ENGINEERS WY,RG,YK	PITCH ANGLE 0°
	DATE 06JA78	BISTATIC ANGLE 0°

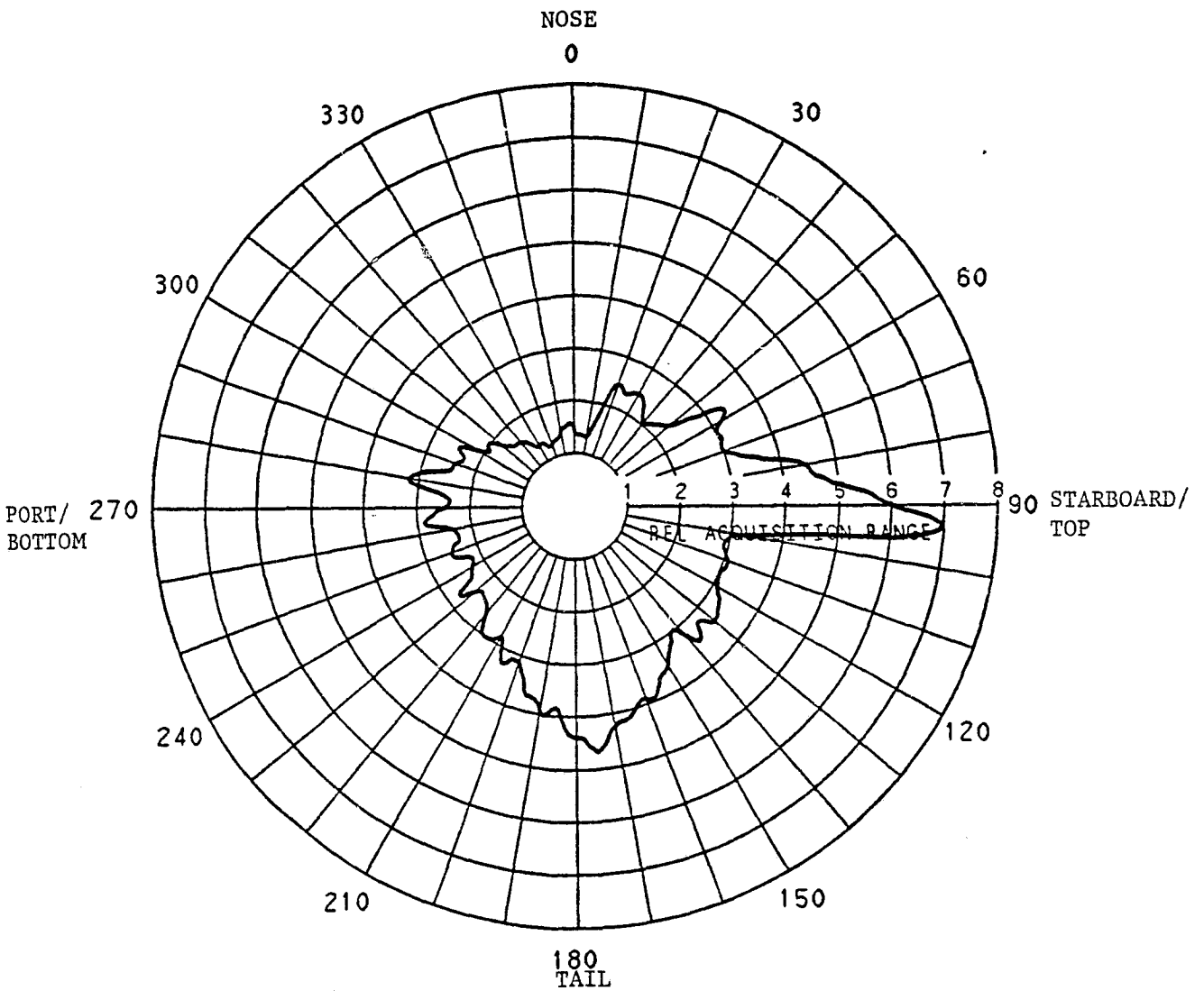

Figure 37. Fourth Root of Median Radar Cross Section of Space Shuttle Orbiter, +50 Degrees Roll Angle.

PACIFIC MISSILE TEST CENTER Point Mugu, California		
PATTERN 78-0015 00	FREQUENCY 6.27 GHz	TILT ANGLE 0°
PROJECT SPACESHUTTLE	POLARIZATION HH	ROLL ANGLE + 60°
TARGET ORBITER	ENGINEERS WY,RG,YK	PITCH ANGLE 0°
	DATE 06JA78	BISTATIC ANGLE 0°

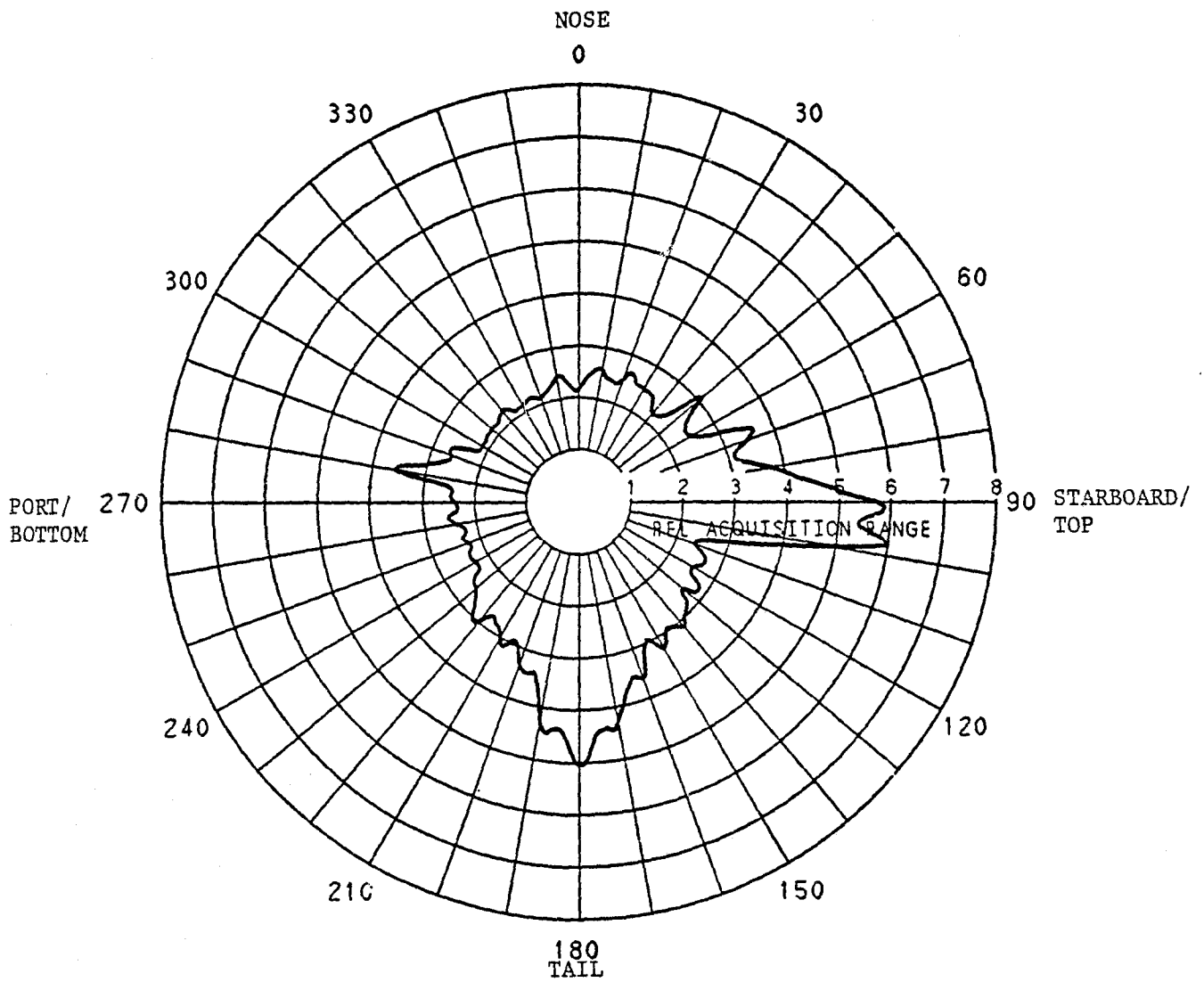

Figure 38. Fourth Root of Median Radar Cross Section of Space Shuttle Orbiter, +60 Degrees Roll Angle.

PACIFIC MISSILE TEST CENTER Point Mugu, California		
PATTERN 78-0016 00	FREQUENCY 6.27 GHz	TILT ANGLE 0°
PROJECT SPACESHUTTLE	POLARIZATION HH	ROLL ANGLE + 70°
TARGET ORBITER	ENGINEERS WY,RG,YK	PITCH ANGLE 0°
	DATE 06JA78	BISTATIC ANGLE 0°

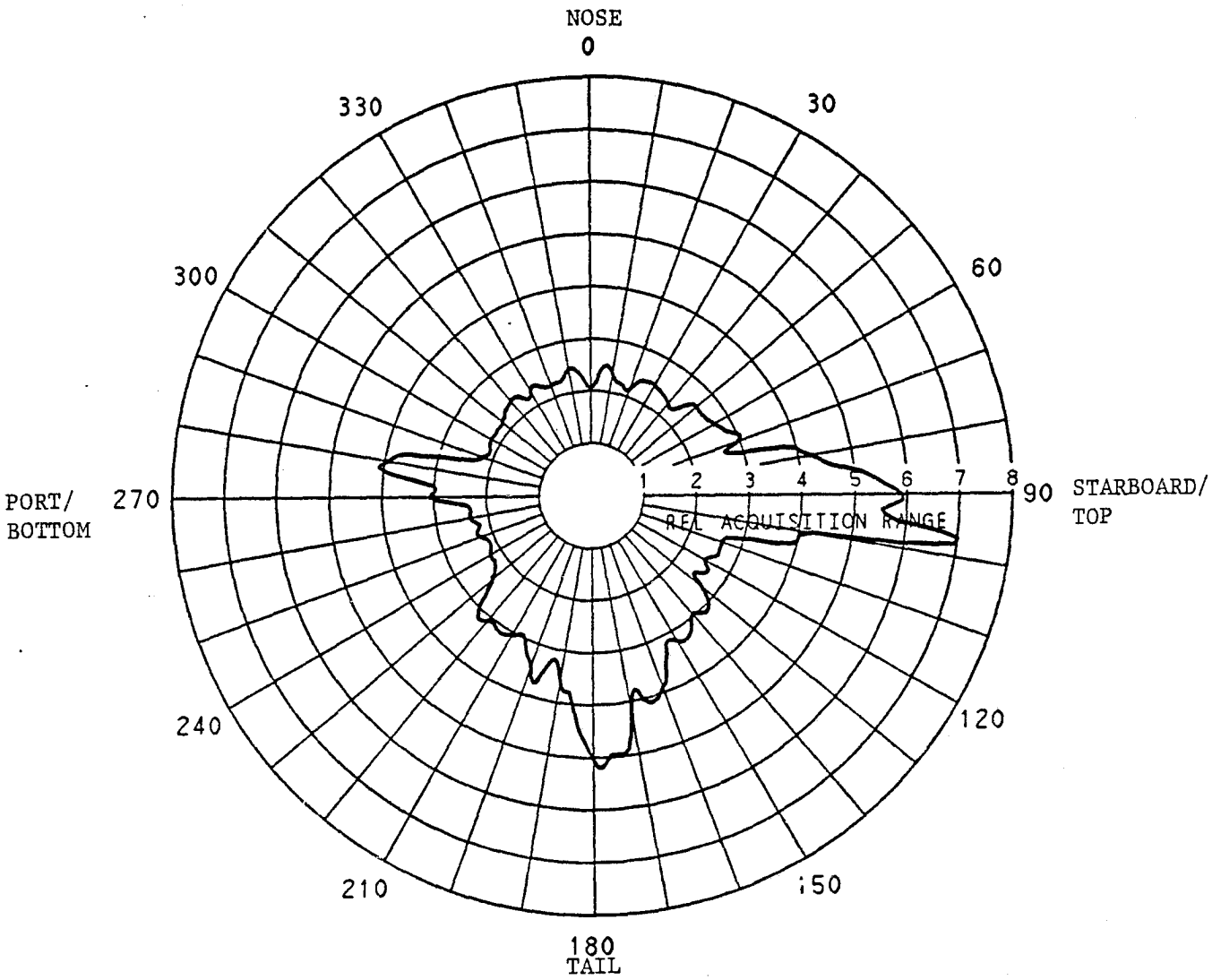

Figure 39. Fourth Root of Median Radar Cross Section of Space Shuttle Orbiter, +70 Degrees Roll Angle.

PACIFIC MISSILE TEST CENTER Point Mugu, California		
PATTERN 78-0018 00	FREQUENCY 6.27 GHz	TILT ANGLE 0°
PROJECT SPACESHUTTLE	POLARIZATION HH	ROLL ANGLE + 80°
TARGET ORBITER	ENGINEERS WY,RG,YK	PITCH ANGLE 0°
	DATE 06JA78	BISTATIC ANGLE 0°

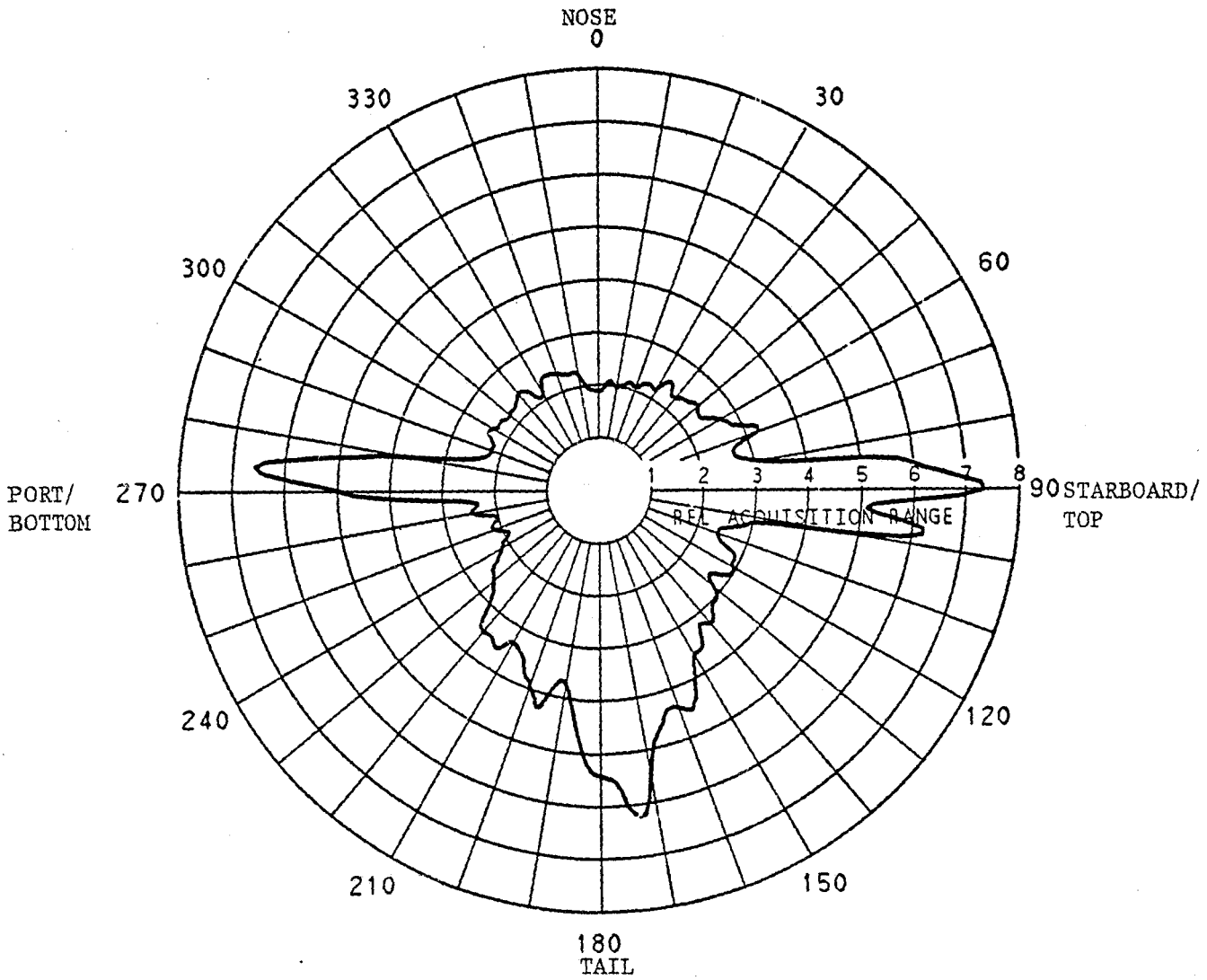

Figure 40. Fourth Root of Median Radar Cross Section of Space Shuttle Orbiter, +80 Degrees Roll Angle.

PACIFIC MISSILE TEST CENTER Point Mugu, California		
PATTERN 78-0017 00	FREQUENCY 6.27 GHz	TILT ANGLE 0°
PROJECT SPACESHUTTLE	POLARIZATION HH	ROLL ANGLE + 90°
TARGET ORBITER	ENGINEERS WY,RG,YK	PITCH ANGLE 0°
	DATE 06JA78	BISTATIC ANGLE 0°

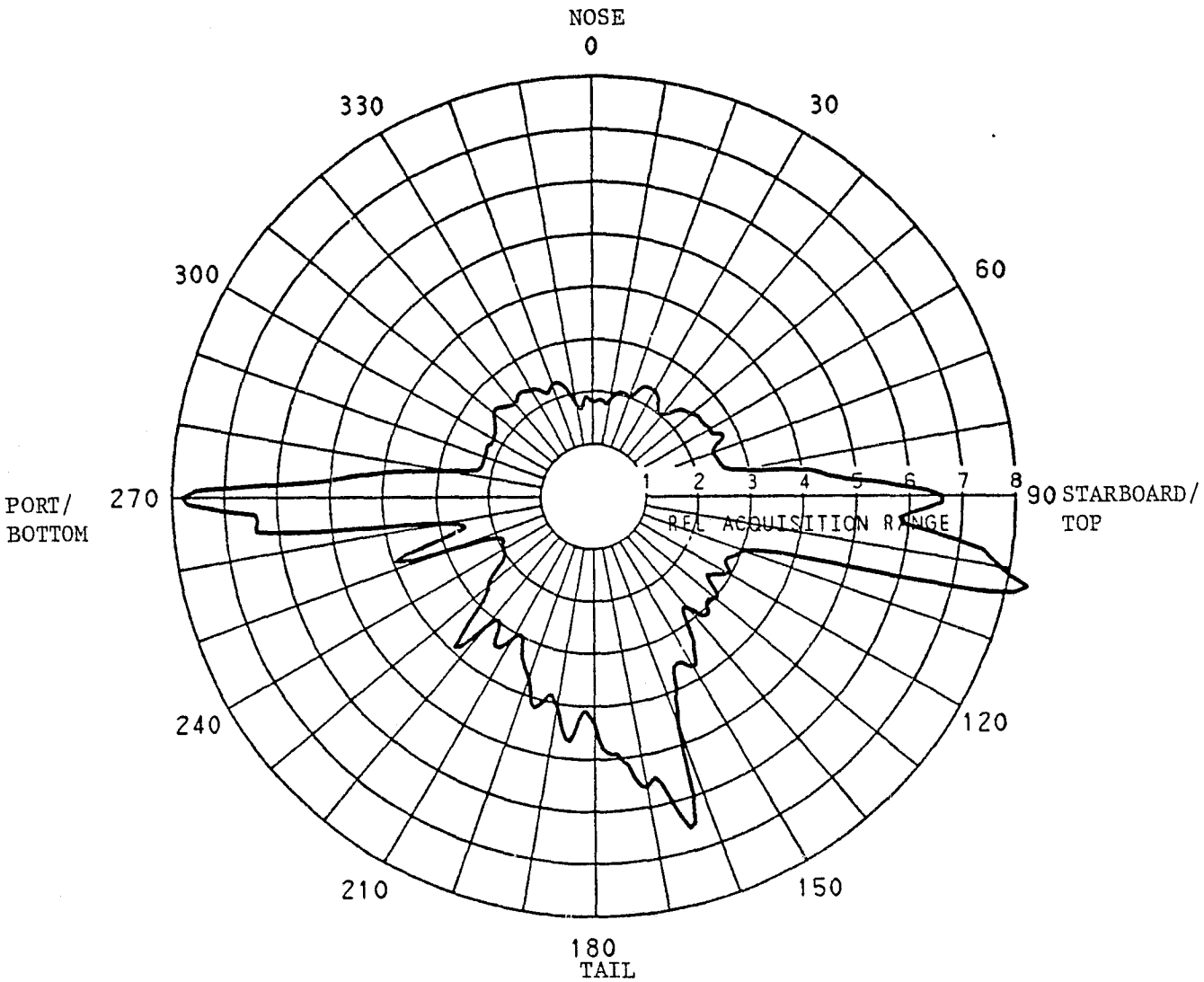

Figure 41. Fourth Root of Median Radar Cross Section of Space Shuttle Orbiter, +90 Degrees Roll Angle.